DEUTSCHES ELEKTRONEN-SYNCHROTRON DESY

DESY 83-042
June 1983

CHARGED PARTICLE AND NEUTRAL KAON PRODUCTION IN e^+e^- ANNIHILATION AT PETRA

by

JADE Collaboration

ISSN 0418-9833

NOTKESTRASSE 85 · 2 HAMBURG 52

To be sure that your preprints are promptly included in the
HIGH ENERGY PHYSICS INDEX ,
send them to the following address (if possible by air mail) :

DESY
Bibliothek
Notkestrasse 85
2 Hamburg 52
Germany

DESY 83-042
June 1983

ISSN 0418-9833

CHARGED PARTICLE AND NEUTRAL KAON PRODUCTION IN e^+e^- ANNIHILATION AT PETRA

JADE Collaboration

W. Bartel, L. Becker, C. Bawbery, D. Cords, R. Eichler[1], R. Felst, D. Haidt,
H. Krehbiel, B. Naroska, J.Olsson, P. Steffen, P. Warming
Deutches Elektronen-Synchrotron DESY , Hamburg, Germany

G. Dietrich, E. Elsen[2], G. Heinzelmann, H. Kado, K. Meier,
A. Petersen, G. Weber
II.Institut für Experimentalphysik der Universität Hamburg, Germany

S. Bethke, A. Dieckmann, J. Heintze, K.H. Hellenbrand,
R.D. Heuer, S. Kawabata[3], S. Komamiya, J. von Krogh, P. Lennert,
H. Matsumura, H. Rieseberg, A. Wagner[4]
Physikalisches Institut der Universität Heidelberg, Germany

A. Finch, F. Foster, G. Hughes, T. Nozaki, H. Wriedt
University of Lancaster , England

J. Allison, A.H. Ball, G. Bamford, R. Barlow, C. Bowdery, I.P. Duerdoth,
I. Glendinning, F.K. Loebinger, A.A. Macbeth, H. McCann, H.E. Mills,
P.G. Murphy, P. Rowe, K. Stephens
University of Manchester , England

D. Clarke, R. Marshall, G.F. Pearce, J B. Whittaker
Rutherford Appleton Laboratory, Chilton , England

J. Kanzaki, T. Kobayashi, M. Koshiba, M. Minowa, M. Nozaki, S. Odaka,
S. Orito, A. Sato, H. Takeda, Y. Totsuka, Y. Watanabe[3], S. Yamada,
C. Yanagisawa[5]
Lab. of Int. Coll. on Elementary Particle Physics
and Department of Physics, University of Tokyo, Japan

[1]now at Labor. f. Hochenergiephysik der ETH-Zürich, Villigen, Switzerland
[2]now at SLAC, Stanford, Calf., U.S.A.
[3]now at KEK, Oho-Machi, Tsukuba-Gun, Ibaraki-Ken, Japan
[4]Heisenberg foundation fellow
[5]now at Rutherford Appleton Laboratory, Chilton, England

ABSTRACT

The mean charged multiplicity as well as its distribution has been measured as a function of c.m. energy in the reaction $e^+e^-\rightarrow$hadrons. Fragmentation models are compared with the data. After applying radiative corrections the mean charged multiplicity is measured to be 8.4 ± 0.3 ± 0.6 at 12 GeV, 13.1 ± 0.3 ± 0.6 at 30 GeV and 13.6 ± 0.3 ± 0.6 at 35 GeV. The ratio of mean charged multiplicity to the dispersion ($\langle N_{ch}\rangle / D_{ch}$) is almost constant in the energy range studied, indicating KNO scaling of the charged multiplicity. The inclusive differential cross section $s(d\sigma/dx_p)$ shows scaling violation in the high x_p region (x_p>0.15). The absolute value of the scaling violation is consistent with the result of 2nd order QCD caluculations. The production of neutral kaons has been investigated by identifying the decay $K_S^0\rightarrow\pi^+\pi^-$. The production probability for a strange quark relative to that of a u or d quark in the fragmentation, γ_s, has been determined to be 0.27 ± 0.03 ± 0.05 averaged over c.m. energies from 12 to 35 GeV. Momentum spectra for neutral kaons are presented and are compared with model predictions.

I INTRODUCTION

Multihadron production in e^+e^- annihilation appears to be the simplest way to study the fragmentation of partons (quarks and gluons) into hadrons. The annihilation process of e^+e^- into a virtual photon as well as the coupling of quarks to the photon is well understood in terms of QED. Furthermore the c.m. energy of the hadronic system is clearly defined in e^+e^- annihilation, except for well understood radiation effects, because all of the incident energy contributes to the creation of particles with no spectators. In lepton-hadron and hadron-hadron collisions, on the other hand, the initial state is a complicated mixture of quarks and gluons, so that the momentum distribution of the constituents must be known before investigating the fragmentation processes.

Investigations of the global jet structure have provided evidence for the basic processes of quantum chromodynamics (QCD) through the observation of multi-jet events[1][2]. Complementary to such QCD studies is the investigation of the fragmentation process itself, which is the subject of this paper[3]. We analyse data obtained with the JADE detector at PETRA in the c.m. energy range from 12.0 GeV to 36.7 GeV.

Results are presented on corrected multiplicity distributions and momentum spectra for both charged particles and neutral kaons.
In fragmentation models, the multiplicity of charged particles is essentially given by the fragmentation function, determining the relative particle momenta along the jet direction, and by the fraction of pseudoscalar to vector particles produced. Experimental constraints on the parameters controlling these model properties are obtained. The determination of the energy dependence of the charged particle momentum distribution makes it possible to investigate the evolution with energy of the fragmentation function. Furthermore models with different fragmentation schemes can be tested by comparing their predictions with the experimentally obtained average multiplicity as well as with its distribution.
The study of neutral kaons supplies additional information. During fragmentation, secondary quark antiquark pairs are produced from the vacuum. Strange quarks appear to be suppressed, relative to u and d quarks, in this process. In order to determine the suppression factor from the K^0 multiplicity the contributions from primary quarks are taken into account. Moreover, possible correlations with other fragmentation parameters which influence the multiplicities are investigated. The experimental momentum spectra of both charged particles and neutral kaons are presented. The consistency of these spectra with the fragmentation parameters obtained in the analysis of multiplicities is investigated.

II EVENT SELECTION

The JADE detector and trigger conditions have been described elsewhere[4]. In the off-line selection of candidate events for the reaction $e^+e^-\rightarrow$ hadrons the following criteria were applied :

(1) The shower energy in the leadglass barrel and endcap counters had to exceed certain thresholds, which varied with the C.M. energy as follows:

barrel part	> 3.0 GeV	
or each end cap	> 0.4 GeV	at $\sqrt{s}$ > 24 GeV
barrel part	> 2.0 GeV	
or each end cap	> 0.4 GeV	at 16 GeV < $\sqrt{s}$ < 24 GeV
barrel part	> 1.2 GeV	
or each end cap	> 0.2 GeV	at $\sqrt{s}$ < 16 GeV

(2) In order to suppress QED and cosmic ray background, at least four tracks were required to come from a cylindrical fiducial volume of radius 30 mm (in the plane perpendicular to the beam, r-φ) and length ±350 mm (beam direction, z) around the interaction point. This volume was chosen to be considerably larger than the size of the interaction region folded with the resolution. Among the tracks, three were required to have transverse momenta greater than 50 MeV/c relative to the beam and to have more than 24 hits out of a maximum of 48 hits per track. $\tau^+\tau^-$ background was further suppressed by rejecting 4 track events if three of the tracks were in the opposite direction to the fourth.

(3) The remaining radiative Bhabha events, having more than three tracks due to γ conversion, were excluded in a visual scan where e^+e^- pairs and secondary electromagnetic showers were recognized using the information from the track detector and the lead glass counters.

A data reduction factor of about 300 was obtained with these criteria. About 50 % of the events accepted by the above criteria are multihadron events from 1γ annihilation. The other events are mainly due to two photon processes. To separate the 1γ annihilation events, cuts were applied in the total visible energy:

$$E_{vis} = \sum_i p_i + \sum_j E_j \quad > \sqrt{s}/2 \,,$$

and in the longitudinal momentum balance:

$$|B_L| = |\sum_i p_i \cos\vartheta_i + \sum_j E_j \cos\vartheta_j| / E_{vis} < 0.4$$

where the p_i are the momenta of the charged particles and the E_j are the energies of shower clusters in the leadglass counters. The ϑ_i and ϑ_j are polar angles.

After these cuts, the estimated background from $\tau^+\tau^-$ events is 1.3 %, and that from two photon processes is about 1 %. The overall detection efficiency and radiative corrections [5] were estimated by Monte Carlo event simulation using the Lund model [6]; including radiative corrections the efficiency $(\varepsilon\cdot(1 + \delta))$[1] is close to one [4],[7]. The number of multihadron events obtained at various C.M. energies is listed in Table 1.

[1] ε is the acceptance for the multihadron events with radiative correction included and $(1 + \delta)$ is the radiative correction factor due to higher order QED processes up to order α^3.

III MULTIPLICITY AND MOMENTUM DISTRIBUTION

FOR CHARGED PARTICLES

Measuring method and corrections for the charged multiplicity

Charged multiplicity distributions have been measured at C.M. energies of 12, 30 and 35 GeV. At each C.M. energy, a subsample of 130 to 200 events was selected from the multihadron sample after applying a further cut on the polar angle ϑ_{th} of the thrust axis, viz.:

$$|\cos\vartheta_{th}| < 0.7 .$$

This cut reduces a possible bias due to particles lost in the beam pipe and decreases the two photon background to 0.3 %.

To determine the number of charged tracks, the events were scanned by physicists using an interactive graphics display program. Basically, tracks found by the pattern recognition program were counted. The aim of the visual inspection was to identify nuclear interactions in front of the jet chamber, to recognize tracks with kinks which were doubly reconstructed by the program and to identify tracks back scattered from the material surrounding the jet chamber.

The counting criteria of the visual scan were:

(1) e^+e^- pairs from photon conversions were rejected. An oppositely charged pair was regarded as a converted photon when the opening angle was consistent with zero within 3σ, as expected from the multiple scattering and track fit errors. In addition, an energetic pair (with one of the tracks having a momentum p greater than 0.8 GeV/c) was considered to be a photon conversion only when the energy deposit in the leadglass counters was more than 70% of the expectation for an e^+e^- pair.

(2) A nuclear interaction in the material in front of the jet chamber, with one or more charged tracks was counted as one charged track.

(3) Tracks with $p_T < 0.05$ GeV/c were rejected, where p_T is the transverse momentum relative to the beam axis.

(4) All the other charged tracks were counted including charged tracks from K_s^0 and Λ decays.

The charged multiplicity distributions obtained with the above criteria are shown in Fig.1.

The observed mean charged multiplicity obtained by the visual scanning is

$$\langle N_{obs} \rangle = 8.39 \pm 0.22 \quad \text{at 12 GeV},$$
$$\langle N_{obs} \rangle = 12.21 \pm 0.25 \quad \text{at 30 GeV},$$
$$\langle N_{obs} \rangle = 12.41 \pm 0.26 \quad \text{at 35 GeV}.$$

Various corrections to the mean charged multiplicity were estimated by visual scanning of the Monte Carlo generated events where the history of the tracks is known.

The corrections are classified as follows:

(1) $\langle N_{out} \rangle$ is the number of charged particles produced but not observed in the volume of the jet chamber. Charged particles going into the beam pipe, as well as K_S^0 and Λ decays outside the jet chamber, are included in this correction.

(2) $\langle N_{low} \rangle$ is the number of charged tracks with $p_T < 0.05$ GeV/c which are emitted into the jet chamber.

(3) $\langle N_{miss} \rangle$ is the number of tracks not reconstructed by the pattern recognition program. The inefficiency occurs mostly from the complete overlap of two tracks in r-φ. The estimate is consistent with the value estimated by the dE/dx measurement in the jet chamber (overlapping tracks have a dE/dx value twice as large as single tracks)[8].

(4) $\langle N_{\gamma \to h} \rangle$ is the number of tracks which actually come from photon conversions but are accepted as real tracks. (This correction is negative.)

(5) $\langle N_{h \to e} \rangle$ is the number of tracks misidentified as e^+ or e^- of photon conversions.

(6) $\langle N_{int} \rangle$ is the number of tracks rejected as secondary particles produced by nuclear interactions, although they are real tracks. This type of misidentification occurs, for example, for tracks which are scattered in the material through a large angle or are produced by K_S^0 decays, and which happen to intersect with other tracks in the material in front of the jet chamber.

(7) $\langle N_{abs} \rangle$ is the number of charged tracks which interact in the beam pipe without emitting any charged particles. The disappearance of charged tracks is mainly caused by charge exchange reactions and absorption with no secondary particles. This value is estimated from the momentum dependent pion-nuclei reaction cross section.

(8) Because of the jet structure of the events, many tracks are close to each other. Therfore, when there are two tracks very close in the material and one of them interacts emitting several charged particles, all the tracks are treated as secondaries, including the track which passes close to the interaction. $\langle N_{close} \rangle$ is the number of tracks misidentified as secondary tracks of this type.

(9) Residual $\tau^+\tau^-$ background is still contained in the multihadron sample (about 1%). Since we rejected 1-3 prong events, most of the remaining $\tau^+\tau^-$ events have 3-3 prongs. $\langle N_\tau \rangle$ is the correction for the $\tau^+\tau^-$ background per event.

These corrections and their errors are listed in Table 2.

The mean charged multiplicity of the multihadron events selected by the standard cuts and the jet axis cut was obtained by applying the above corrections, with the following result:

$$\langle N_{corr} \rangle = 9.04 \pm 0.26 \quad \text{at 12 GeV},$$
$$\langle N_{corr} \rangle = 13.22 \pm 0.27 \quad \text{at 30 GeV},$$
$$\langle N_{corr} \rangle = 13.50 \pm 0.29 \quad \text{at 35 GeV}.$$

To estimate the systematic uncertainty of the corrections, two sets of Monte Carlo simulated events were generated and visually scanned, one using the Lund model[6] and the other using the model by Hoyer et al.[9]. The sum of the corrections (1) to (9) is essentially independent of the two models and depends mainly on the detector performance.

In order to determine the charged multiplicity of the hadron system at a C.M. energy of exactly $\sqrt{s}$ (without initial state radiation), one must add the corrections due to the rejection of events by the standard multihadron selection including the thrust axis cut and due to the initial state radiation effect. Since the charged multiplicity distributions of the models are different, the following correction is model dependent. For the correction the Lund model was used.

(10) $\langle N_{cut} \rangle$ is the difference between the mean charged multiplicity of Monte Carlo generated events without initial state radiation and of those with initial state radiation[5] selected by the cuts. The cor-

rection is almost independent of the maximum energy of the initial state radiation k_{max}, if k_{max} is large enough. In the simulation we used $k_{max}=0.99 \cdot E_{beam}$.

After applying correction (10) the mean charged multiplicity at $\sqrt{s}$ is

$$\langle N_{ch} \rangle = 8.4 \pm 0.3 \pm 0.6 \quad \text{at 12 GeV,}$$
$$\langle N_{ch} \rangle = 13.1 \pm 0.3 \pm 0.6 \quad \text{at 30 GeV,}$$
$$\langle N_{ch} \rangle = 13.6 \pm 0.3 \pm 0.6 \quad \text{at 35 GeV.}$$

The systematic errors include contributions of 0.3 for visual scanning bias.

In order to be able to compare with other experiments, we subtract the secondaries from K_S^0 and Λ as well as leptons from heavy quark weak decays and from Dalitz decays. Thus we obtain for the mean charged multiplicity of hadrons with life time greater than 10^{-9} sec (the sum of $\pi^{\pm}$, $K^{\pm}$, p and $\bar{p}$):

$$\langle N_{had} \rangle = 7.2 \pm 0.5 \pm 0.7 \quad \text{at 12 GeV,}$$
$$\langle N_{had} \rangle = 11.4 \pm 0.4 \pm 0.7 \quad \text{at 30 GeV,}$$
$$\langle N_{had} \rangle = 11.8 \pm 0.4 \pm 0.7 \quad \text{at 35 GeV.}$$

Details of this last correction are given in Table 3. Secondary tracks resulting from nuclear interactions of neutral hadrons such as K_L^0 and neutrons are negligible because the mean number of K_L^0 per event is only 0.5 to 0.8 and that of n ($\bar{n}$) is much less. Furthermore, their probability to interact with subsequent emission of charged particles is only a few percent. The value is in good agreement with the TASSO result 11.9±0.5 at 34 GeV[12][13].

Energy dependence of the mean charged multiplicity

Recently it was observed at PETRA that the increase of the mean charged multiplicity with s was much faster than logarithmic[4][14]. Combining our results on the mean charged multiplicity with the data from other experiments[14][15] (see Fig.2), the s-dependence was fitted to each of the following functions :

$$\langle N_{ch} \rangle = a + b \cdot \ln(s) \quad \text{(a)}$$
$$\langle N_{ch} \rangle = a + b \cdot (\ln(s))^2 \quad \text{(b)}$$
$$\langle N_{ch} \rangle = a + b \cdot \ln(s) + c \cdot (\ln(s))^2 \quad \text{(c)}$$
$$\langle N_{ch} \rangle = a \cdot s^b \quad \text{(d)}$$
$$\langle N_{ch} \rangle = a + b \cdot \exp[c \sqrt{\ln(s/\Lambda^2)}] \quad \text{(e)}$$
$$\langle N_{ch} \rangle = a + b \cdot \exp[c \sqrt{\ln(s/\Lambda^2) \ln\ln(s/\Lambda^2)}] \quad \text{(f)}$$

where a,b and c are free parameters and the QCD scale parameter Λ was fixed to 0.3 GeV. The resulting values of the parameters as well as the χ^2 per degree of freedom are given in Table 4. In combining the data from various e^+e^- experiments, statistical and systematic errors were summed linearly at each data point in the fit.

Except for the logarithmic function (a), which results from the Feynman scaling hypothesis[16], all functions describe the data well. The functions (b) and (c) were proposed because their s-dependence is faster than logarithmic. The power law (d) was predicted for e^+e^- annihilation in fireball and hydrodynamical models[17]. These functions fit the data reasonably well up to and including the PETRA energy region. Note that a quadratic polynomial in ln(s) also fits the charged multiplicity in $p\bar{p}$ collisions, up to the SPS collider energies of $\sqrt{s}$ = 540 GeV[18], though with different parameters. The function (e) is obtained by perturbative QCD calculations[19]. A good fit was also obtained when the parameter c was fixed at 1.7, as expected by QCD in next-to-leading order[20]. The function (f) was predicted by a different QCD calculation[21] with non-leading effects. There is no significant difference between (e) and (f). At higher energies the functions predicted by QCD calculations increase much faster than the functions (b), (c) and (d). In addition to the functions investigated above the data were also compared with the predictions of fragmentation models. This will be discussed in the next section.

Fragmentation models

We have studied two fragmentation models including hard gluon emission and investigated how well they can reproduce the observed charged multiplicities. In the Lund model[6], the fragmentation takes place along the colour string stretched between the partons. In the model by Hoyer et al.[9], the axes of fragmentation are just the momentum vectors of the partons. In both models, the production of hadrons is controlled by a number of free parameters, to be adjusted to the data. The strong coupling strength α_s and the mean transverse momentum of secondary quarks σ_q have been obtained in previous studies of the global properties of multi-jet events[2][22][23][24]. The values used in this analysis are $\alpha_s = 12\pi/(23\cdot\ln(s/\Lambda^2))$ with $\Lambda = 0.3$ ($\alpha_s = 0.17$ for $\sqrt{s} = 34$ GeV) and $\sigma_q = 0.35$ GeV/c. The remaining essential parameters are:

- γ_s, the probability of producing an $s\bar{s}$ pair from the vacuum relative to that of $u\bar{u}$ production. For the analysis of the multiplicity and the charged momentum spectra, we fix $\gamma_s = 0.3$, which is consistent with the K^0 analysis presented in section 4.
- r, the fraction of pseudoscalar mesons relative to the sum of pseudoscalar and vector mesons produced in the fragmentation.
- the parameter entering the primordial fragmentation function f(z).

Since the two models differ in the details of the fragmentation functions used, we will now discuss both models in turn:

The Lund model uses the function $f(z) = (1 + \beta)\cdot(1 - z)^\beta$ with β a free parameter for u and d quarks. The corresponding β values for heavier quarks were fixed at 0.35 for s, 0.15 for c and 0.05 for b. f(z) vanishes for z = 1, taking into account soft gluon effects. The parameters β and r are strongly correlated, for a given charged multiplicity. This is expected since the multiplicity can be increased both by softening the fragmentation function and by increasing the relative fraction of vector mesons. In Fig. 3 the contour lines in the β-r plane are given, for various values of the mean charged multiplicity $\langle N_{ch}\rangle$. The shaded band is that region allowed by the mean multiplicity. This is done for the c.m. energies $\sqrt{s}$ = 12, 30, and 35 GeV. It is clear from the figures that r and β cannot be determined simultaneously from a multiplicity measurement alone. Following Field-Feynman[25], we choose r = 0.5 and obtain the following values for β:

$\beta = 0.20^{+0.28}_{-0.20}$ at $\sqrt{s}$ = 12 GeV

$\beta = 0.64^{+0.12}_{-0.12}$ at $\sqrt{s}$ = 30 GeV

$\beta = 0.53^{+0.13}_{-0.11}$ at $\sqrt{s}$ = 35 GeV,

where the errors are statistical only. The systematic errors can be read from Fig. 3. For fixed r, the values of the exponent β in the fragmentation function are compatible with increasing with energy. A variation with Q^2 of the fragmentation function has been predicted in the frame work of QCD[26]. It has been caluculated for e^+e^- annihilations in ref.(27) in analogy to the Q^2-evolution of the parton momentum distribution function in deep inelastic lepton nucleon interaction[28]: Once the fragmentation function is defined at some Q_0^2, its Q^2-evolution can be calculated. The results of these calculations are illustrated in Fig. 4a where f(z) = 1 has been defined at $\sqrt{s}$ = 5 GeV. The fragmentation function is shown in the figure for four different values of $\sqrt{s}$. As can be seen, QCD tends to soften f(z), due to increased emission of gluons.

In order to include a Q^2 evolution of the fragmentation function in the Lund model, we parametrise the s-dependence of the β through the empirical relationship[2]

$$\beta(s) = 0.018\cdot\sqrt{s}$$

which is consistent with the experimental β values obtained above. Fig. 4b shows the curves for $(1+\beta)\cdot(1 - z)^\beta$ with β given by the above relation, for the same $\sqrt{s}$-values as in Fig. 4a. Except for very small z values, the s-dependent β-parameter simulates well the s-dependence expected from QCD, in the energy range covered by this experiment.

The prediction for the charged multiplicity of the Lund model with energy dependent β are compared in Fig. 2 with data at all energies. At energies above 10 GeV the data are well described by the model. At lower energies the data from SLAC-LBL and Frascati rise slower than the model prediction. Note, however, the the LENA point at 7 GeV fits the model well. The strong rise of $\langle N_{ch}\rangle$ at PETRA energies cannot be attributed to $b\bar{b}$ production alone. According to the Lund model its contribution is only 0.4 ± 0.1 (the error is due to uncertainty in the fragmentation function of the b-quark). In this model the decay multiplicity of the bottom mesons is optimized to fit the data from the lowest lying bottom meson ($\langle N_{ch}$/B-meson$\rangle$ = 5.75 ± 0.1 ± 0.2) which was measured by the CLEO group at the upsilon (4S) resonance[29].

The model by Hoyer et al. has been investigated in a similar manner. The fragmentation function is given by

$$f(z) = 1 + a_F + 3\cdot a_F\cdot(1-z)^2$$

---

[2] For the generation of the Monte Carlo events used in this analysis we used the parametrisation $\beta(s) = 0.015\cdot\sqrt{s}$, which is based on an earlier investigation.

with a_F being a free parameter[25]. As before, the mean charged multiplicity was used to determine the parameter a_F, again with r fixed at 0.5:

$a_F = 0.30 \pm 0.12$ at $\sqrt{s} = 12$ GeV
$a_F = 0.48 \pm 0.06$ at $\sqrt{s} = 30$ GeV
$a_F = 0.46 \pm 0.06$ at $\sqrt{s} = 35$ GeV.

Hence this model can also be successfully adjusted to describe the mean multiplicity.

Charged multiplicity distribution

In order to obtain the true distribution of the charged multiplicity from the observed one, the probability (ε_{ij}) of observing i particles when j particles are produced was estimated by visually scanning the simulated events. In determining the ε_{ij}, only the effects due to the detector performance (corrections (1)-(9)) were considered, so that the ε_{ij}'s are essentially independent of the two models considered. The number of events with original multiplicity j (n(j)) can be obtained by solving the set of simultaneous equations.

$$m(i) = \sum_j \varepsilon_{ij}\, n(j)$$

where m(i) is the number of events with observed multiplicity i. Since n(j) is zero for odd numbers of j because of charge conservation, the set of equations is highly constrained. Therefore the n(j)'s were obtained by using the least squares method, minimizing the value

$$\sum_i \Big(m(i) - \sum_j \varepsilon_{ij} \cdot n(j) \Big)^2$$

As a result, the n(j)'s are solutions of the set of simultaneous equations

$$\sum_i \sum_j (\varepsilon_{ik} \cdot \varepsilon_{ij}) n(j) = \sum_i \varepsilon_{ik} \cdot m(i)$$

In Fig. 5 the corrected distributions are shown and compared with the predictions from the Lund model and the model by Hoyer et al.. For each model the parameters in the fragmentation functions have been optimized by fitting the mean charged multiplicity. No further adjustments were made. Since correction (10) is model dependent, the distributions in Fig.5 are corrected only for effects (1) to (9). On the other hand, the

multihadron selection cuts were applied to the simulated events which includes the initial photon radiation. The distributions predicted at 30 and 35 GeV by the Lund model agree very well with the data, in contrast to the model by Hoyer et al. Whereas the latter model could be successfully adjusted to fit the mean charged multiplicity, it fails to describe in the shape of the distribution, predicting distributions much broader than the experimental ones. Further attempts to simultaneously adjust, in the latter model, the parameters r and a_F in order to fit the average charged multiplicity as well as the width of its distribution were not successful. The charged multiplicity distribution predicted by a model in which the Lund (string) fragmentation scheme is used, but where the primordial fragmentation function is the Field-Feynman function[25], lies between the predictions of the two original models, as shown in Fig.5(c). This implies that the difference in the distributions from the two models originates not only from the different primordial fragmentation functions, but also from their fragmentation schemes. As previously reported[30], the particle density in the angular regions between jets is also described better by the Lund model than by the model of Hoyer et al. Further analysis is based mainly on the Lund model.

In Fig.6, the inverse of the relative dispersion $\langle N_{ch}\rangle/D_{ch}$ as a function of $\sqrt{s}$, is given together with data from PLUTO and LENA[31]. Here D_{ch} is defined by

$$D_{ch} = \sqrt{\langle N_{ch}^2\rangle - \langle N_{ch}\rangle^2}\ .$$

Our measurements give the following results:

$\langle N_{ch}\rangle/D_{ch} = 2.86 \pm 0.25$ (at 12 GeV),
$\langle N_{ch}\rangle/D_{ch} = 3.05 \pm 0.16$ (at 30 GeV),
$\langle N_{ch}\rangle/D_{ch} = 3.20 \pm 0.15$ (at 35 GeV).

In QCD parton cascade models, the emission of a gluon, in general, changes the colour of the radiating parton. Thus successive emissions are not independent. Such theories predict that the ratio $\langle N_{ch}\rangle/D_{ch}$ is asymptotically constant with a value of about three[32]. Although the errors are large, the data are consistent with that prediction. For the case of a simple Poisson distribution, the quantity $\langle N_{ch}\rangle/ D_{ch}^2$ is expected to be constant. This can be ruled out. The result obtained from the Lund model also fit the data well. As discussed before, a broader distribution is obtained from the model by Hoyer et.al..

$\langle N_{ch}\rangle/D_{ch} = 3.24$ (Lund 35 GeV),
$\langle N_{ch}\rangle/D_{ch} = 2.76$ (Hoyer 35 GeV).

KNO scaling

It has been argued that, for given multiplicity N, the expression $\langle N\rangle\cdot\sigma_N/\sigma_{tot}$ is a function only of $N/\langle N\rangle$ and the deviation is $O(1/\ln(s))$, where σ_N is the cross section for producing N particles[33]. This property is expressed by the KNO equation:

$$\langle N\rangle\cdot\sigma_N/\sigma_{tot} = \psi(N/\langle N\rangle)$$

where $\psi(N/\langle N\rangle)$ is a scaling function. The KNO plot obtained from the corrected charged multiplicity distribution n(j) is shown in Fig.7. The result is consistent with KNO scaling within the errors.
The data were fitted by the function[34]

$$\psi(z) = C\cdot z^{\alpha}\cdot\exp(-B\cdot z^{\beta})$$

where

$$C = 2\beta\left\{\Gamma[(\alpha+2)/\beta]^{2(\alpha+1)/\beta}\right\}/\left\{\Gamma[(\alpha+1)/\beta]^{2(\alpha+1)/\beta+1}\right\}$$

$$B = \{\Gamma[(\alpha+2)/\beta]/\Gamma[(\alpha+1)/\beta]\}^{2}$$

As shown in Fig.7, the KNO function fits the data quite well, with the parameters of the best fit given by $\alpha = 3.68 \pm 0.39$ and $\beta = 1.97 \pm 0.11$.

Momentum distribution and scaling violation

The inclusive differential cross section $s(d\sigma/dx_p)$ ($x_p = p/p_{beam}$) for charged particles without identification of the particle type was obtained from the momentum spectrum, corrected for detection efficiency and initial state radiation.

In events selected by the standard multihadron cuts and the thrust axis cut mentioned before, tracks were used for obtaining the inclusive cross section if they satisfied

(1) $p_T > 0.1$ GeV/c, where p_T is the momentum component perpendicular to the beam;

(2) The number of hits in the r-φ track reconstruction is not less than 16;

(3) $R_{min} < 7.0$ mm, where R_{min} is the distance of the closest approach to the beam in r-φ. $|z_0| < 350$ mm, where z_0 is the intercept of the track at r=0 in the z-r plane. This cut was optimized to reduce background from secondary nuclear interactions in the material in front of the chambers.

Before applying any other corrections, the momentum spectrum was corrected for effects due to the finite momentum resolution. Since the systematic momentum error contains contributions from many sources, some of which are not completely understood, we corrected the distribution by using experimentally observed quantities only: the measured curvature c_k and its error Δc_k of each track k. The correction was done for each bin in x_p in the following way. For each track k, the resolution function $g_k(x_p)$ was defined assuming a Gaussian distribution in the curvature c, the mean value and the width of which were assumed to be given by the experimental value c_k and Δc_k respectively. The probability density function of the original x_p distribution for the track k, $f_k(x_p)$, was approximated by convoluting $g_k(x_p)$ with the observed distribution dN/dx_p and normalizing in the region $0 < x_p < 1$:

$$f_k(x_p) = g_k(x_p)\cdot(dN/dx_p)_{obs}/\left(\int_0^1 g_k(x_p)\cdot(dN/dx_p)_{obs}\,dx_p\right)$$

The corrected number of entries in the i-th bin of x_p was then obtained by integrating $f_k(x_p)$ over the i-th bin and summing up the contributions from all tracks:

$$N_i = \sum_k \int_{\text{bin i}} f_k(x_p)dx_p$$

The method used was tested by model calculations on distributions with similar slopes as the x_p-distribution, smeared with a known resolution. The method was found to reproduce the original distribution satisfactorily as long as the width of the resolution function was comparable in magnitude to the bin width, which in the present experiment is the case for $x_p < 0.6$. In order to estimate the systematic error of the correction, $f_k(x_p)$ was also approximated by convoluting $g_k(x_p)$ with distributions obtained from fragmentation models, which led to similar results.

In addition to correcting for the momentum smearing effect, a correction was made for the contamination from τ pair production ($\approx$ 1.3 % of all events). The correction is about 1 % at $x_p = 0.1$, increasing to 3-4 % at $x_p > 0.4$. The background from two photon processes ($\approx$ 0.3 % of all events) was neglected.
The differential cross section in bin i is then obtained from the corrected number of events N_i by

$$s(d\sigma/dx_p)|_{corr.} = s \cdot (N_i - B_i) / \{\varepsilon_i \cdot \Delta_i \cdot L \cdot \varepsilon'(1+\delta) \} \cdot f_i,$$

Here B_i is the number of background tracks in bin i, ε_i is the detection efficiency of charged particles in bin i, Δ_i is the width of the x_p bin i, L is the integrated luminosity, and f_i is the radiative correction factor.

The detection efficiency for the multihadron events $\varepsilon'(1+\delta)$ after the standard multihadron cuts and the jet axis cut including radiative corrections was 0.66±0.02 at 35 GeV.

The detection efficiency ε_i for charged particles in the selected multihadron events was obtained by Monte Carlo detector simulation, which includes γ conversions, multiple scattering, energy loss in the material and double track resolution in the jet chamber. Due to the third selection criterion discussed at the biginning of the section, the detection efficiency including track reconstruction efficiency was about 90 % above 1 GeV/c. It decreases to 70 % at 0.3 GeV/c mainly due to multiple scattering. f_i is a factor for correcting the shape of the x_p distribution which is distorted through the effects of initial state radiation. This correction is typically 2 %, increasing to 5 % at very high x_p.

The loss of tracks due to interactions in front of the chambers was estimated from the momentum dependent nuclear interaction cross sections[35]. This correction is almost constant at high momenta (5 % for > 1 GeV/c) and about 10 % at ≈ 0.3 GeV/c due to resonance formation. The luminosity was obtained from the number of Bhabha events in the barrel part of the lead glass counters.

The error of $s(d\sigma/dx_p)$ contains the systematic error of the corrections due to detection efficiency (~ 4 %), nuclear interactions (~ 1 % above 1 GeV/c, 3 % at ≈ 0.3 GeV/c), and the momentum smearing effect (< 1 % for x_p<0.4 and ~ 20 % at x_p = 0.8). The systematic error for the absolute normalisation was estimated to be 4 %.

Fig. 8. shows the inclusive differential cross section $s\cdot(d\sigma/dx_p)$, for c.m. energies of 14 and 35 GeV. For x_p larger than 0.15 the cross section for $\sqrt{s}$ = 35 GeV is observed to be approximately 20 % smaller than that for $\sqrt{s}$ = 14 GeV. This scaling violation is reproduced by the Lund model with the energy dependent fragmentation function, the predictions of which agree well with the data at both energies, in the range $0.15 \leq x_p \leq 0.4$. For x_p values larger than 0.4 the model predictions for both energies lie above the data. This is possibly due to the shape of the fragmentation function assumed in the model.

The scaling violation is further studied in Fig. 9 where the ratio $(s\cdot d\sigma/dx_p(35\ GeV))/(s\cdot d\sigma/dx_p(14\ GeV))$ is plotted as a function of x_p, together with data from TASSO[36]. The ratio of cross sections has the advantage that the error of the overall normalisation does not enter. The two experiments agree very well with each other, both indicating a scaling

violation of about 20 % for $x_p \geq 0.15$. Also shown is the prediction of the Lund model with a constant fragmentation function $(1 - z)^\beta$ with $\beta = 0.5$. It leads, by hard gluon emission, to a scaling violation of only about 10 %, half as large as observed experimentally. Agreement with the data is significantly improved if the phenomenological energy dependent fragmentation function, as discussed above, is used, the prediction of which is also given in Fig. 9. Note that most of the scaling violation originates from the evolution with $\sqrt{s}$ of the fragmentation function. A scaling violation as large as 20% has also been obtained by Peterson et al.[37] using a second order perturbative quark jet evolution model.

Fig. 10 shows the scaling cross section averaged over various x_p bins as a function of the c.m. energy, together with the corresponding TASSO data. The data can be fitted well with a function $a\cdot(1 + b\cdot\ln(s))$. The resulting fit values for the parameters a and b are given in Table 5.

Recently it was found[38] that a fragmentation function harder than that used in the Lund model describes best the fragmentation of the charm and bottom quarks. Calculations using such harder functions show that the model predictions discussed above change by only a few percent and hence the same conclusions are reached.

Before closing this section we recall that, in the analysis of the charged multiplicity above, it was found that the fragmentation parameters r and β are strongly correlated and could not be determined simultaneously. We note here that this ambiguity cannot be resolved by the additional constraint of the momentum distribution since the momentum-distribution hardly changes for r and β values obtained by moving along the region in the r-β plane allowed by the charged multiplicity measurement. A more direct determination of the parameter r, however, is possible by measuring the vector mesons produced[3]. We study this in a subsequent paper.

---

[3] TASSO deduced a value for r of 0.42 ± 0.08 ± 0.15 from the number of ρ^0's with 0.2 < x < 0.7 at 34 GeV[39]. Note that in their analysis, the value of the parameter r was deduced by comparing the observed number of ρ^0's with the predictions of the model by Hoyer et al., for various values of r, however at a fixed value of a_r.

IV NEUTRAL KAON PRODUCTION

Identification of the decay $K_S^0 \to \pi^+\pi^-$

In the sample of multihadron events, a search was made[3] for the decay $K_S^0 \to \pi^+\pi^-$. It was identified by the invariant mass of pairs of oppositely charged tracks.

In order to reduce combinatorial background, only those tracks satisfying the following criteria were used to compute the invariant mass:

(A) The number of hits used in the r-φ track reconstruction is not less than 24 out of a maximum of 48 hits;

(B) Tracks from identified photon conversions are excluded;

(C) The tracks must have $|z_0| < 350$ mm, where z_0 is the intercept of the track at r=0 in the z-r plane;

(D) The tracks must not come from the interaction point, taking into account the fit and multiple scattering errors in r-φ:

$R_{min} > 3 \cdot \sigma_{Rmin}$ and $R_{min} > 4$ mm at $E_{CM} > 20$ GeV

$R_{min} > 2 \cdot \sigma_{Rmin}$ and $R_{min} > 3$ mm at $E_{CM} < 20$ GeV

where R_{min} is the minimum distance of the track to the beam in the r-φ plane and σ_{Rmin} is the error expected from multiple scattering and track fitting;

(E) The tracks must have momenta larger than 0.1 GeV/c.

After thus selecting good tracks in each event, the r-φ vertex points of all the oppositely charged pairs were calculated. The K_S^0 mass resolution is dominated by the resolution in the opening angle, which is mainly determined by the accuracy of the z-measurement. The z coordinate is measured by the charge division method in the jet chamber. In order to improve the mass resolution a refitting of the tracks in the z-r plane was carried out for each track using a least square method. In simultaneously fitting the two tracks in the z-r plane, a constraint was imposed that both tracks had the same z at the decay vertex, which is accurately determined in the r-φ plane. After performing z-r fitting, further geometrical cuts were applied on the decay vertex position to avoid background from nuclear interactions in the material in front of the chambers, viz:

$$10 \text{ mm} < l < 120 \text{ mm} \quad \text{or} \quad l > 200 \text{ mm}$$

$$\chi^2 = (d/\sigma_d)^2 < 5$$

where l is the decay length in the r-φ plane, d is the distance between the reconstructed flight path and the beam in the r-φ plane and σ_d is the r.m.s. spread in d expected from multiple scattering and track fitting. For each selected pair, a correction was made for the energy loss of particles in the material in front of the chambers and the invariant mass was calculated assuming the charged pion mass for each track. The mass distributions are shown in Fig.11. The residual background originates mainly from nuclear interactions and was estimated from like-charged pairs. As a check, the decay time distribution was obtained from the reconstructed K_S^0 and is shown in Fig.12 for C.M. energy 35 GeV. It agrees well with the table value for the K_S^0 lifetime. A typical candidate for K_S^0 decay is shown in Fig.13.

The momentum-dependent detection efficiency for the $K_S^0 \to \pi^+\pi^-$ decay was estimated from a Monte Carlo simulation. Multihadron events were generated according to the Lund model and treated in the JADE detector in the same way as real data. The detection efficiency is shown in Fig.14 as a function of K_S^0 momentum. The systematic error in the detection efficiency was estimated by variation of the fragmentation parameters in the model simulation and by changing the cut parameters of the $K_S^0 \to \pi^+\pi^-$ selection. It is momentum dependent and varies from negligible values at small momenta to about 20 % of the detection efficiency above 6 GeV/c including the statistical errors of the Monte Carlo calculation.

Inclusive momentum spectrum and number of neutral kaons per event

The inclusive differential cross section $d\sigma/dp$ for neutral kaons was obtained at 12, 14, 22, 30 and 35 GeV. The spectrum was corrected[40] for the detection efficiency, for the $K_S^0 \to \pi^+\pi^-$branching fraction and by a factor 2 due to equal production probabilities of K_S^0 and K_L^0. The systematic errors in the differential cross section originate from the uncertainty in the detection efficiency, in the luminosity, and in the background subtraction. The systematic error in the luminosity was less than 3 %. The systematic error from the background subtraction was less than 5 % in the momentum range above 1.0 GeV/c and about 15 % in the range below 0.5 GeV/c. Finally, the spectrum was corrected for effects due to initial state radiation. The differential cross section for various C.M. energies is shown in Fig.15, together with results from the TASSO experiment[41] and from model simulations using the Lund model. Fig.16 shows the same data plotted in terms of the Lorentz invariant cross section. At lower C.M. energies

of about 4-5 GeV, this distribution can be well described by a simple exponential $a \cdot \exp(-b \cdot E)$ [42], as expected from thermodynamical arguments. As can be seen from Fig.16, this is not the case at PETRA energies. In the low momentum region the data deviate significantly from an exponential distribution.

Data obtained at different C.M. energies are best compared using the scaling cross section $(s/\beta)\cdot(d\sigma/dx_E)$ with $x_E = E/E_{beam}$. This is done in Fig.17[43][41][44]. From the low energy of the MARK-I experiment[43] to our highest energy of 35 GeV, the data are compatible with the Feynman scaling hypothesis in the region $x_E > 0.2$ but do not exclude a scaling violation of the order of 30 %.

The number of neutral kaons per event was obtained by integrating the momentum spectrum. For this the number of neutral kaons with momenta greater than 10 GeV/c was estimated using the Lund model. The correction was about 1.8 % at $\sqrt{s}$ = 35 GeV. The resulting numbers are:

1.14 ± 0.27 ± 0.11	at 12 GeV
1.05 ± 0.10 ± 0.11	at 14 GeV
1.27 ± 0.16 ± 0.13	at 22 GeV
1.49 ± 0.22 ± 0.15	at 30 GeV
1.45 ± 0.08 ± 0.15	at 35 GeV

The average number of kaons increases with C.M. energy as shown in Fig.18(a) together with results from other experiments[43][44][45][46][13]. Also shown in this figure is the contribution to neutral kaons production expected from the weak decays of heavy quarks as well as from primary strange quarks. Whereas at lower C.M. energies this is the dominant source of for neutral kaons, at energies far above the bottom threshold most of the neutral kaons originate from the fragmentation process. The inclusive cross section of neutral kaons relative to the point like muon pair production cross section

$$R(K^0,\bar{K}^0) = (\sigma(K^0) + \sigma(\bar{K}^0))/\sigma_{\mu\mu}$$

was obtained at each energy by multiplying the numbers given above by the R value of the total multihadron production at that energy[7] (Fig.18(b)):

$R(K^0,\bar{K}^0)$ = 3.86 ± 0.96 ± 0.39	at 12 GeV,
4.06 ± 0.41 ± 0.44	at 14 GeV,
5.13 ± 0.66 ± 0.55	at 22 GeV,
5.62 ± 0.85 ± 0.59	at 30 GeV,
5.74 ± 0.32 ± 0.62	at 35 GeV.

Origins of neutral kaons and

determination of the fragmentation parameter γ_s

In e^+e^- annihilation, the neutral kaons originate from three sources:
(1) primary strange quarks,
(2) strange quarks from weak decays of charm or bottom quarks,
(3) secondary strange quarks from fragmentation.
As discussed in the last section, the increase of the number of neutral kaons with C.M. energy is due to the increase of the number of strange quarks from the fragmentation.

In the fragmentation, the production probability of an $s\bar{s}$ pair relative to that of $u\bar{u}$ or $d\bar{d}$ is denoted by γ_s. As far as the strong interaction alone is concerned, the quark production probability is independent of charge and flavour but is a function of the quark mass. If the mass of the s-quark were equal to that of the u-quark or the d-quark, γ_s would be 1.

In order to experimentally determine γ_s, a systematic study of possible correlations between γ_s and other fragmentation parameters was made using the Lund model. Fig.19 shows the average number of neutral kaons versus the mean charged multiplicity expected from the Lund model while varying the parameters r and γ_s through certain discrete values. Here r is the fraction of pseudoscalar mesons relative to the sum of pseudoscalar and vector mesons produced in the fragmentation. Whereas the mean charged multiplicity strongly increases inversely with r, the average number of neutral kaons per event is rather independent of this parameter and is essentially given by γ_s. This effect can be easily understood as follows: An increase of the K^* yield relative to the pseudoscalar kaons does not change the number of neutral kaons in the final state. On the other hand, an increase of ρ and ω relative to π and η increases the number of charged pions from the decay products.
A similar study is made in Fig.20 with the parameter β in the Lund primordial fragmentation function which phenomenologically describes soft gluon effects. By varying the parameter β, only a small change in the number of neutral kaons is obtained.

As seen above, the parameter γ_s is largely insensitive to r and β and is determined by the number of neutral kaons. A comparison of the experimental number of neutral kaons with the predictions of the Lund model leads to

γ_s = $0.37^{+0.37}_{-0.21}$ at 12 GeV,

= $0.26^{+0.12}_{-0.10}$ at 14 GeV,

= $0.28^{+0.12}_{-0.10}$ at 22 GeV,

= $0.29^{+0.13}_{-0.11}$ at 30 GeV,

= $0.26^{+0.06}_{-0.06}$ at 35 GeV.

Here the systematic error due to uncertainties of r and β is included. There is no indication of energy dependence of γ_s in the PETRA energy range. The average value is $\gamma_s = 0.27 \pm 0.03 \pm 0.05$. This agrees well with the value 0.29 ± 0.02 from neutrino experiments[47] and with the value 0.3 ± 0.1 from hadron-hadron interactions[48], but is lower than the value 0.5 originally proposed by Field and Feynman[25].

V SUMMARY

We have measured charged particle multiplicities at C.M. energies of 12, 30 and 35 GeV. The mean charged multiplicity rises faster than logarithmically as a function of the C.M. energy. It can be satisfactorily fitted by functions predicted by perturbative QCD. Fragmentation models based on first order QCD also give a good description of the energy dependence of the mean charged multiplicity. Whereas the Lund model describes as well the distribution of the charged multiplicity, the model by Hoyer et al. fails in this respect at C.M. energies above 30 GeV. The charged multiplicity distribution exhibits KNO scaling. The inclusive differential cross section $s(d\sigma/dx_p)$ of charged particles exhibits scaling violation at large x_p (x_p>0.15). The absolute value of the scaling violation is consistent with the 2nd order QCD calculation. There is a trend in the behaviour of the averaged multiplicity with C.M. energy as well as of the x_p distribution of charged particles which can be explained with an energy dependent fragmentation function.

The inclusive production of neutral kaons was studied at C.M. energies from 12 to 35 GeV. The Lorentz invariant cross section at high C.M. energies does not show the simple exponential behaviour observed around $\sqrt{s}$ = 5 GeV. A comparison of the scaling cross section in the energy range from 5 to 35 GeV shows that the data, in the region x > 0.2, are compatible with Feynman scaling but would also allow a scaling violation of the order of 30 %. The average number of neutral kaons per event varies from 1.1 at $\sqrt{s}$ = 14 GeV to 1.5 at $\sqrt{s}$ = 35 GeV. At 14 GeV approximately 1/2 of the neutral kaons can be accounted for by the production of $s\bar{s}$ pairs from the vacuum during the fragmentation. This fraction rises to 2/3 at 35 GeV. The production probability of an $s\bar{s}$ pair relative to a $u\bar{u}$ pair in the fragmentation has been determined to be $0.27 \pm 0.03 \pm 0.05$ averaged over C.M. energies from 12 to 35 GeV, which is lower than originally proposed by Field and Feynman.

We are indebted to the PETRA machine group for their excellent support and to all the engineers and technicians who have participated in the construction and maintenance of the apparatus. This experiment was supported by the Bundesministerium für Forschung und Technologie, by the Educational Ministry of Japan and by the UK Science Research Council through the Rutherford Laboratory. The visiting groups wish to thank the DESY directorate for their hospitality.

REFERENCES

1) TASSO Collaboration, R. Brandelik et al , Phys. Lett. 86B(1979)243

MARK J Collaboration, D.P. Barber et al , Phys. Rev. Lett. 43(1979)830

PLUTO Collaboration, Ch. Berger et al., Phys. Lett. 86B(1979)418

JADE Collaboration, W. Bartel et al., Phys. Lett. 91B(1980)142

W. Braunschweig, Int. Symp. on Lepton and Photon Interactions at High Energy, Bonn, Germany (1981) p. 68

2) JADE Collaboration, W. Bartel et al., Phys. Lett. 115B(1982)338

3) This paper is based on the Ph.D. thesis by S. Komamiya (UTLICEPP-82-01, LICEPP Faculty of Science, University of Tokyo).

4) JADE Collaboration, W. Bartel et al., Phys Lett. 88B(1979)171

5) F.A. Berends and R. Kleiss, DESY 80/66 (1980)

F A. Berends and R. Kleiss, DESY 80/73 (1980)

6) T. Sjöstrand and B. Söderberg, LU-TP 78-18 (1978)

B. Anderson et al., Z. Physik C1(1978)105

B. Anderson and G. Gustafson, Z. Physik C3(1980)223

T. Sjöstrand, LU-TP 80-03 (1980)

B. Anderson et al., LU-TP 81-03 (1981)

T. Sjöstrand, LU-TP 82-03 (1982)

7) Precise measurement of total cross section for the process e^+e^-→hadrons in the cm energy range between 12.0 and 36.4 GeV, JADE- Collaboration, in preparation

8) JADE Collaboration, W. Bartel et al., Z. Physik C6(1980)295

9) H. Hoyer et al., Nucl. Phys. B161(1979)349

H. Hoyer et al., DESY 79/21 (1979)

10) 12 and 30 GeV: MARK J and PLUTO Collaborations,

35 GeV: JADE and MARK J Collaborations,

XXth Int. Conf. on High Energy Physics, Madison, U.S.A. (1980) p. 593

11) JADE Collaboration, W. Bartel et al. Phys. Lett. 104B(1981)325

TASSO Collaboration, R. Brandelik et al., Phys. Lett. 105B(1981)75

12) TASSO Collaboration, R. Brandelik et al., DESY 82-070

13) TASSO Collaboration, Dipromarbeit by M. Dittmar, DESY F1-82-03

14) TASSO Collaboration, R. Brandelik et al., Phys. Lett. 89B(1979)418

15) C. Bacci et al., Phys. Lett. 86B(1979)234

J.L. Siegrist, Ph.D. thesis, SLAC-225 (1979)

PLUTO Collaboration, Ch. Berger et al., Phys. Lett. 81B(1979)410

16) R.P. Feynman, Phys. Rev. Lett. 23(1969)1415

17) For a comparison of the predictions for the multiplicity of various phenomenological models see

H. Satz, Current Induced Reactions. p.49, vol 56, Springer-Verlag(1976)

18) W.T. Thome et al., Nucl. Phys. B129(1977)365

K. Alpgard et al., Phys. Lett. 107B(1981)315

19) K. Konishi, Rutherford Lab. RL 79-035 (1979)

W. Furmanski et al., Nucl. Phys. B155(1979)253

A Bassaeto et al., Nucl. Phys. B163(1980)477

20) A.H. Mueller et al., Columbia Univ. CU TP 197 (1981)

21) S. Wada, Phys. Lett. 95B(1980)426

22) S. Yamada, XXth Int. Conf. on High Energy Physics, Madison, U.S.A. (1980) p.616

G. Wolf, rapporteur's talk, XXIIth Int. Conf. on High Energy Physics, Paris, France (1982)

23) W. Bartel et al., DESY 82-060 (1982), to be published

24) JADE results as discussed by W. Braunschweig in reference 1

25) R.D. Field and R.P. Feynman , Nucl. Phys. B128(1977)1

26) H. Georgi and H.D. Politzer, Nucl. Phys. B136(1978)136

H.J. Buras, Review of Mod. Phys. 52(1980)199

G. Altarelli, Physics Report 81(1982)1

27) A. Ali et al., Phys. Lett. 93B(1980)155

28) J.D. Gross, Phys. Rev. Lett. 32(1974)1071

29) CLEO Collaboration,M.S. Alam et al., Phys. Rev. Lett. 49(1982)357

30) JADE Collaboration, W. Bartel et al., Phys. Lett. 101B(1981)129

Evidence for fragmentation along the colour flux lines in 3-jet events, JADE- Collaboration, in preparation

31) PLUTO Collaboration, Ch. Berger et al., Phys. Lett. 81B(1979)410

LENA Collaboration, DESY 81-008 (1981)

32) S. Wolfram, CALT-68-778 (1980)

K. Konishi et al., Nucl. Phys. B157(1979)45

33) Z. Koba, H.B. Nielsen and P. Olesen, Nucl. Phys. B40(1972)317

34) S. Barshay and Y. Yamaguchi, Phys. Lett. 51B(1974)376

S. Barshay, Aachen preprint (1982)

35) B.W. Allardyce et al., Nucl. Phys. A209(1973)1

A.S. Clough et al., Nucl. Phys. B76(1974)15

36) TASSO Collaboration, R.Brandelik et al., Phys. Lett. 114B(1982)65

MARK-II Collaboration, J.F. Patrick et al., Phys. Rev. Lett. 49(1982)1232

37) C. Peterson et al., Phys. Rev. D27(1983)105

38) CDHS Collabolation, H. Abramowicz et al., Z. Physik C15(1982)19

MARK-II Collaboration, J.N. Yelton et al., Phys. Rev. Lett. 49(1982)430

TASSO Collaboration, M. Althoff et al., DESY 83-010

CLEO Collaboration, C. Bebek et al., CLEO 82-01

39) TASSO Collaboration, R.Brandelik et al., Phys. Lett. 117B(1982)135

40) The differential cross section for momentum bin i is given by

$$(d\sigma/dp)_i = \{N(+-)-N(bkg)\}/\{\varepsilon_i \cdot \Delta_i \cdot L \cdot \varepsilon(1+\delta)\} \cdot f_i,$$

where N(+-) is the number of observed oppositely charged pairs in bin i, N(bkg) is the number of background combinations estimated from like charged pairs in bin i, ε_i is the detection efficiency of the neutral kaons in bin i (corrected by branching ratio of $K_S^0 \to \pi^+\pi^-$ and a factor 2 for K_L^0), Δ_i is the width of the momentum bin i, L is the integrated luminosity obtained from the number of Bhabha events in the barrel leadglass counters, and f_i is the radiative correction factor.

41) TASSO Collaboration, R.Brandelik et al., Phys. Lett. 94B(1980)91

TASSO Collaboration, R.Brandelik et al., Phys. Lett. 105B(1981)75

42) DASP Collaboration, R. Brandelik et al., Nucl. Phys. B148(1979)189

43) MARK-I Collaboration, V. Lüth et al., Phys. Lett. 70B(1977)120

44) PLUTO Collaboration, Ch. Berger et al., Phys. Lett. 104B(1981)79

45) MARK-II Collaboration, J. Dorfan, SLAC-PUB 2813(1982)

46) CLEO Collaboration, A. Brody et al., Phys. Rev. Lett. 48(1982)1070

47) P.K. Malhatra and R. Orava, Fermilab-Pub 82/79(1982)

V. Ammosov et al., Phys. Lett. 93B(1980)210

N. Schmitz, Proc. Int. Conf. on Lepton and Photon (1979)359

48) V.V. Anisovich and V.M. Shekhter, Nucl. Phys. 55B(1973)455

A. Suzuki et al., Lett. Nuovo Cimento 24(1979)449

D. Drijard et al., CERN/EP 81-12 (1981)

FIGURE CAPTIONS

FIG. 1 Charged multiplicity distributions obtained by visual scanning

(a) at 12 GeV,

(b) at 30 GeV,

(c) at 35 GeV.

FIG. 2 Energy dependence of the mean charged multiplicity. In this figure, only the statistical errors are shown. Decay products of K_S^0 are included. The curve is obtained using the Lund model.

FIG. 3 Allowed region in the plane of fragmentation parameters β and r, at c.m. energies 12, 30 and 35 GeV. The full lines are the contour for various values of the mean charged multiplicity $\langle N_{ch} \rangle$ as obtained with the Lund model. The shaded band is the region allowed by the experimental value of $\langle N_{ch} \rangle$ (statistical error). The systematic uncertainty is indicated by the dashed lines.

FIG. 4 a) Evolution with $\sqrt{s}$ of the fragmentation function f(z), due to QCD, from references 25 and 26. $f(z) = 1$ has been defined at $\sqrt{s} = 5$ GeV. b) Corresponding curve $f(z) = (1 + \beta)\cdot(1 - z)^{\beta}$, with β given by the empirical relationship $\beta = 0.018\cdot\sqrt{s}$.

FIG. 5 Corrected charged multiplicity distributions for the events which satisfy the standard multihadron selection and the thrust axis cut. The corrections (1) - (9) of chapter III have been applied. Predictions for the Lund model and for the model by Hoyer et al. are also shown. The parameters in the primordial fragmentation functions are optimized so as to obtain the same mean charged multiplicity as the data. (a), (b) and (c) show the distributions at 12 GeV, 30 GeV and 35 GeV respectively.

FIG. 6 Energy dependence of $\langle N_{ch} \rangle / D_{ch}$, where D_{ch} is the dispersion of the charged multiplicity distribution, together with data from the PLUTO and LENA collaborations.

FIG. 7 KNO plot of the charged multiplicity distribution. The data were corrected by using the Lund model. Also shown is the fit with the KNO function of ref. 31.

FIG. 8 Inclusive momentum distribution $s(d\sigma/dx_p)$ ($x_p = p/p_{beam}$) of charged particles without particle identification. The Lund model

curves shown are those obtained with the same parameters used for the predictions in Fig.5. The cross section was corrected for efficiency and for initial state radiation.

FIG. 9 The ratio of $s(d\sigma/dx_p)$ at 35 GeV and those at 14 GeV. Full curve is the prediction of the Lund model with energy dependent β (0.52 at 35 GeV and 0.21 at 14 GeV). Dotted curve is for the same β (= 0.5) at 35 and 14 GeV.

FIG.10 Averaged cross section of $s(d\sigma/dx_p)$ in certain x_p bins. The curves are results of fitting the JADE data by a function $a\cdot(1 + b\cdot\ln(s))$. Note that for the highest x_p range the JADE points are averaged over $0.5 < x_p < 0.6$ whereas the TASSO cover the range $0.5 < x_p < 0.7$.

FIG.11 Invariant mass distribution of oppositely charged tracks satisfying the selection criteria described in the text. Correction for energy loss was made and pion masses were assumed. The width of the peak obtained by a gaussian fit is 17.3 MeV/c^2 (σ) at 14 GeV and 21.3 MeV/c^2 (σ) at 35GeV.

FIG.12 Decay time distribution in units of the K_S^0 life time for $K_S^0\to\pi^+\pi^-$ decay after background subtraction. The straight line is the expectation for the nominal K_S^0 life time τ_0.

FIG.13 A typical candidate for $K_S^0\to\pi^+\pi^-$ decay in the beam pipe. The jet chamber hits and fitted trajectories are shown.

FIG.14 Detection efficiency for the $K_S^0\to\pi^+\pi^-$ decay. The efficiency is limited by the decay length cut at low momentum and by the R_{min} cut at high momentum, where R_{min} is the minimum approach distance from the beam to the track in the r-φ plane.

FIG.15 Radiatively corrected differential cross section $d\sigma/dp$ for neutral kaons.

For 35 GeV (Fig. 15 d), the contributions from primary strange quarks and weak decays of c or b quarks are given. The effect of varying the fragmentation parameter γ_s is also indicated.

FIG.16 Invariant cross section for neutral kaons $(1/4\pi p)(d\sigma/dE)$

FIG.17 Scaling cross section for neutral kaons $(s/\beta)(d\sigma/dx)$, where $x = E/E_{beam}$

(a) data from JADE for various cm energies

(b) data from TASSO, PLUTO and Mark I

FIG.18 (a) $\sqrt{s}$ dependence of the number of neutral kaons per event with data from other experiments[13][41][42][43][45]. Systematic errors are included except for the PLUTO data.

(b) $\sqrt{s}$ dependence of the inclusive cross section for neutral kaons relative to the muon pair pointlike cross section
$R(K^0,\bar{K}^0) = (\sigma(K^0) + \sigma(\bar{K}^0))/\sigma_{\mu\mu}$
with data from other experiments[40][41][42][43][45]. In the plot, systematic errors are included.

When the C.M. energy reaches the threshold of open charm or open bottom, contributions from weak decays of the heavy quarks are switched on. In the energy region far above the bottom threshold, most of the neutral kaons come from the fragmentation processes.

FIG.19 The average number of neutral kaons versus the mean charged multiplicity for three c.m. energies showing the variation of the fragmentation parameters γ_s and r. The point with the error bars indicate the region obtained from the experimentally determined number of neutral kaons and the average charged multiplicity. The dashed error bars indicate the quadratic sum of the systematic errors and the statistical errors.

FIG.20 Same as Fig. 19, for variation of the parameters β and γ_s (with r = 0.5).

TABLE 1

Number of multihadron events selected with the cuts described in the text

$\sqrt{s}$ (GeV)	Number of events
12.0	224
14.0	2649
22.0	1871
27.2 - 32.0	1080
33.0 - 36.9	9616

TABLE 2

Corrections for the mean charged multiplicity

Item	12.0 GeV	30.0 GeV	35.0 GeV
$\langle N_{out} \rangle$	0.30±0.04	0.45±0.05	0.46±0.06.
$\langle N_{low} \rangle$	0.06±0.02	0.09±0.02	0.09±0.03.
$\langle N_{miss} \rangle$	0.06±0.02	0.09±0.02	0.11±0.03.
$\langle N_{e^+e^-} \rangle$	-0.30±0.05	-0.50±0.05	-0.54±0.05.
$\langle N_{h^+e^-} \rangle$	0.24±0.03	0.36±0.04	0.38±0.04.
$\langle N_{int} \rangle$	0.05±0.02	0.07±0.02	0.10±0.03.
$\langle N_{abs} \rangle$	0.13±0.07	0.15±0.09	0.15±0.09.
$\langle N_{close} \rangle$	0.06±0.02	0.14±0.03	0.17±0.03.
$\langle N_{\gamma} \rangle$	0.05±0.02	0.16±0.06	0.17±0.06.
$\sum(1)$-(9)	0.65±0.11	1.01±0.14	1.09±0.15.
$\langle N_{out} \rangle$	-0.52±0.14	-0.10±0.14	0.05±0.14.

TABLE 3

Background for the mean charged multiplicity

Item	$\sqrt{s}$ GeV	12.0	30.0	35.0
$e^{\pm}$ from Dalitz decays		0.08±0.01	0.13±0.01	0.14±0.01
$e^{\pm}$ $\mu^{\pm}$ from heavy hadron weak decays		0.17±0.12	0.19±0.04	0.15±0.04
$\pi^{\pm}$ from K^0_S decays		0.78±0.19	1.03±0.15	1.07±0.11
$\pi^{\pm}$ and $p,\bar{p}$ from $\Lambda,\bar{\Lambda}$ decays		0.24±0.06	0.37±0.10	0.37±0.10

The number of π^0 and η^0 are estimated by using the Lund model with the best fitted parameters.

The number of muons with momenta greater than 2 GeV/c is obtained from data[10]. The number is extrapolated to all momenta by using the Lund model and simply multiplying by two (for electrons).

The number of K^0_S is discussed in section IV.

The number of $\Lambda,\bar{\Lambda}$ is obtained from data[11].

TABLE 4

function	parameters			χ^2/N_{DF}
	a	b	c	
(a)	1.392±0.099	1.180±0.033		3.25
(b)	2.894±0.063	0.190±0.005		0.67
(c)	3.224±0.164	-0.268±0.108	0.229±0.016	0.59
(d)	2.237±0.050	0.243±0.005		0.81
(e)	2.337±0.183	0.016±0.006	2.120±0.122	0.55
(e)	1.630±0.088	0.057±0.002	1.7(fixed)	0.72
(f)	2.254±0.145	0.117±0.031	0.982±0.856	0.56

TABLE 5

x_p	a	b
0.05-0.10	17.3 ± 0.4	0.036 ± 0.004
0.10-0.20	10.4 ± 0.2	-0.038 ± 0.003
0.20-0.30	5.16 ± 0.07	-0.064 ± 0.002
0.30-0.40	2.54 ± 0.04	-0.075 ± 0.003
0.40-0.50	1.01 ± 0.02	-0.071 ± 0.004
0.50-0.60	0.64 ± 0.01	-0.089 ± 0.004

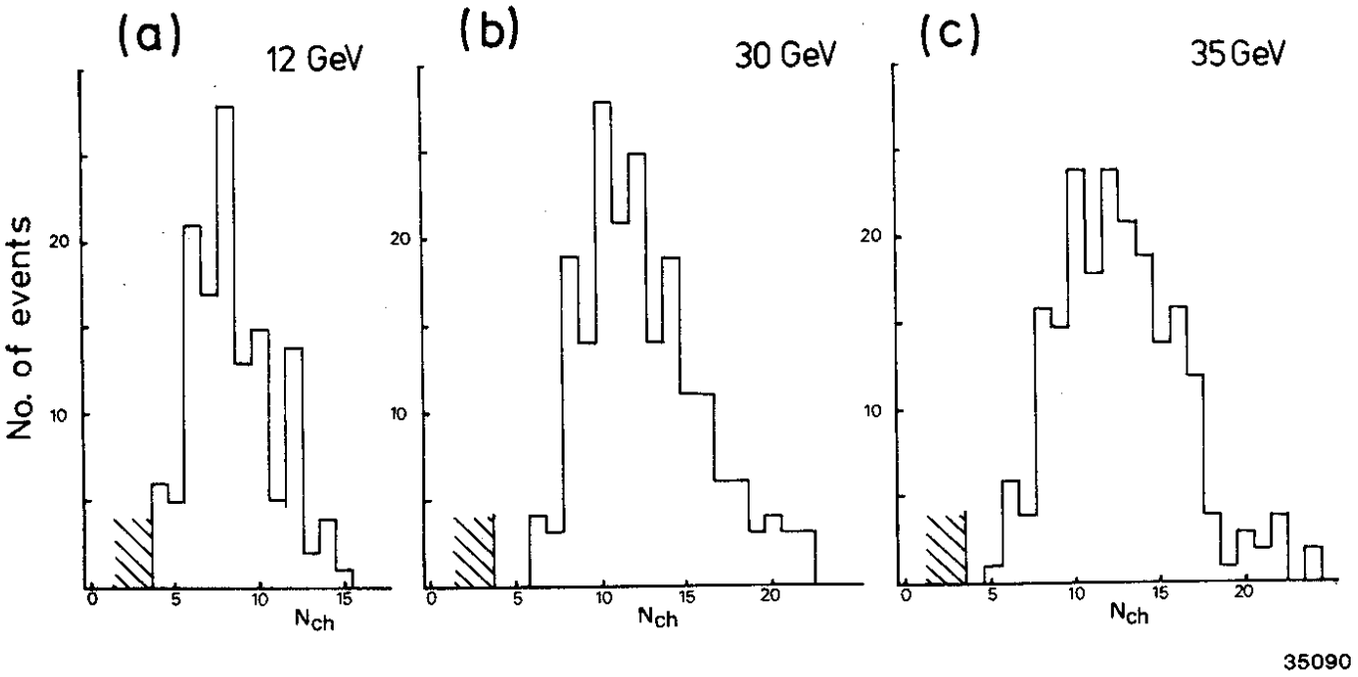
(a)
12 GeV
(b)
30 GeV
(c)
35 GeV
No. of events
N_{ch}
35090

Fig.1

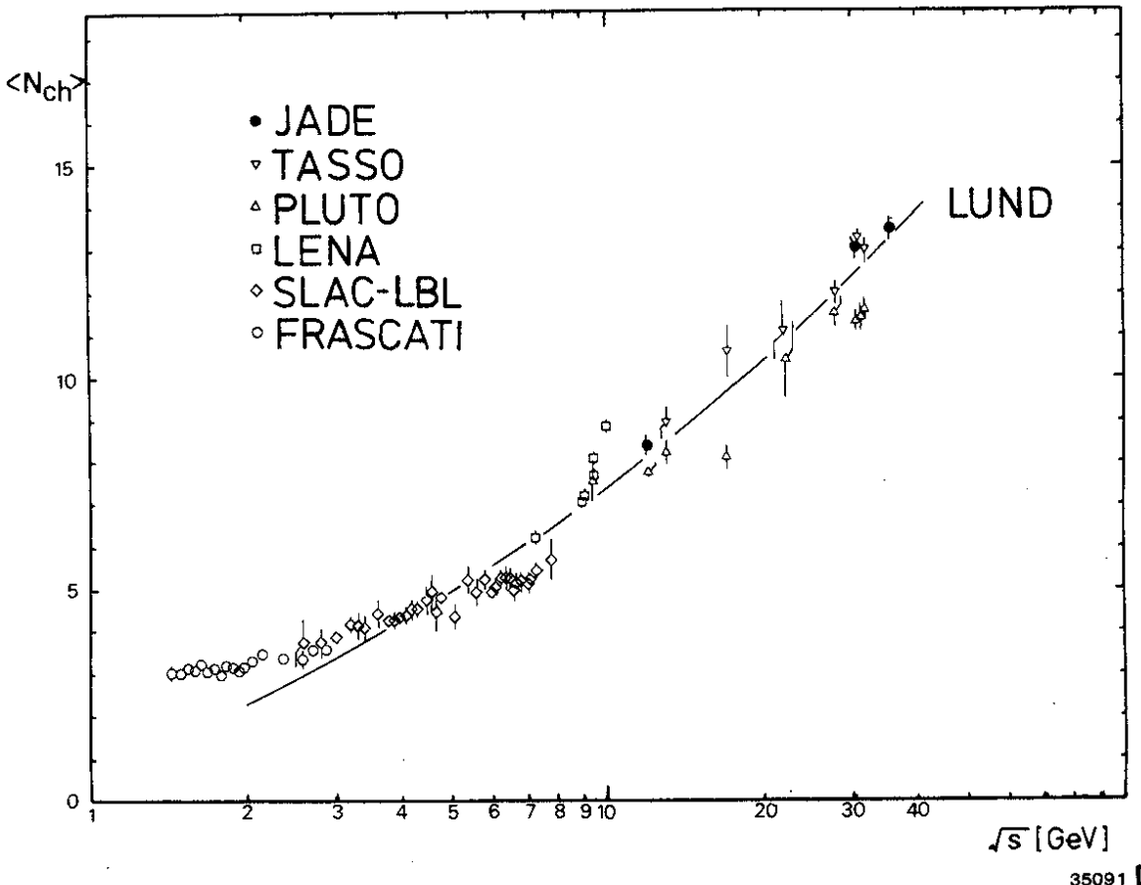
$\langle N_{ch} \rangle$
• JADE
▿ TASSO
△ PLUTO
□ LENA
◇ SLAC-LBL
○ FRASCATI
LUND
$\sqrt{s}$ [GeV]
35091

Fig.2

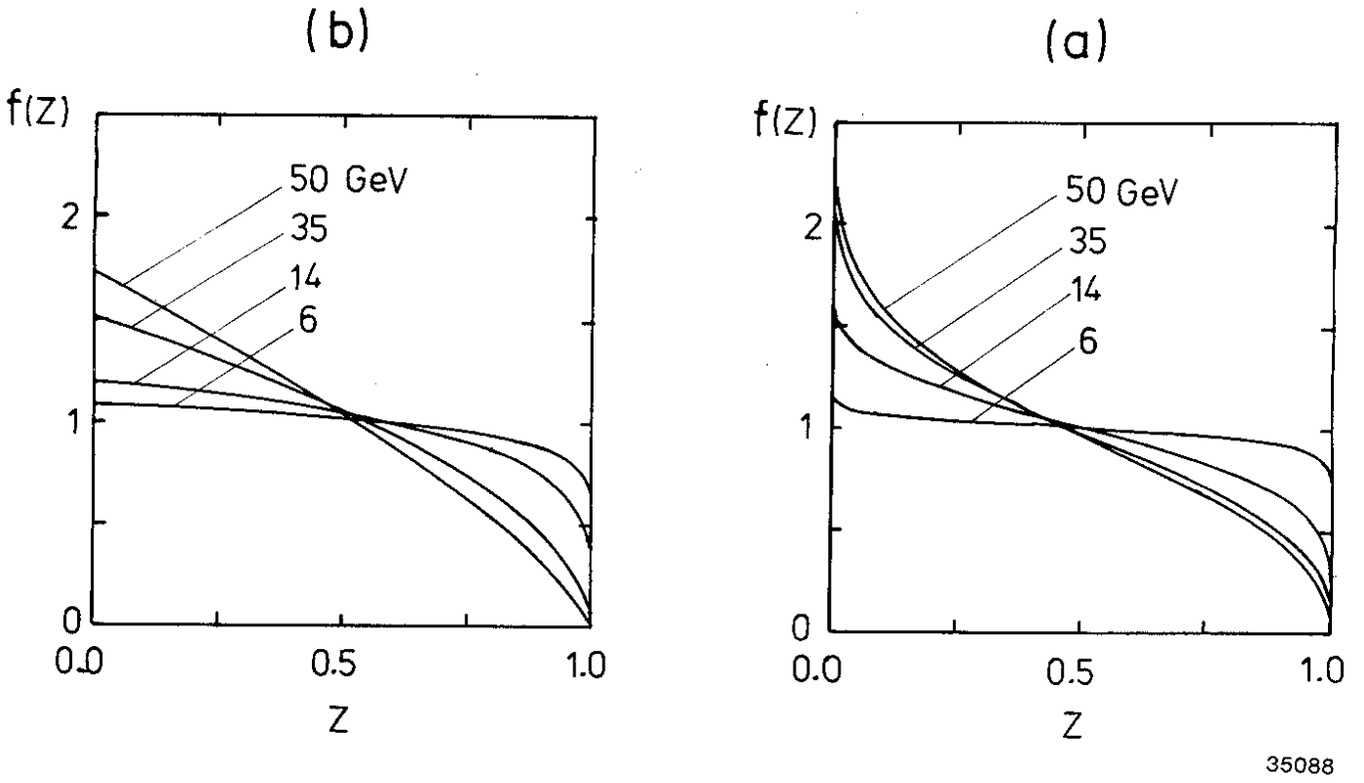
(b)
f(Z)
50 GeV
35
14
6
2
1
0
0.0
0.5
1.0
Z
(a)
f(Z)
50 GeV
35
14
6
2
1
0
0.0
0.5
1.0
Z
35088

Fig. 4

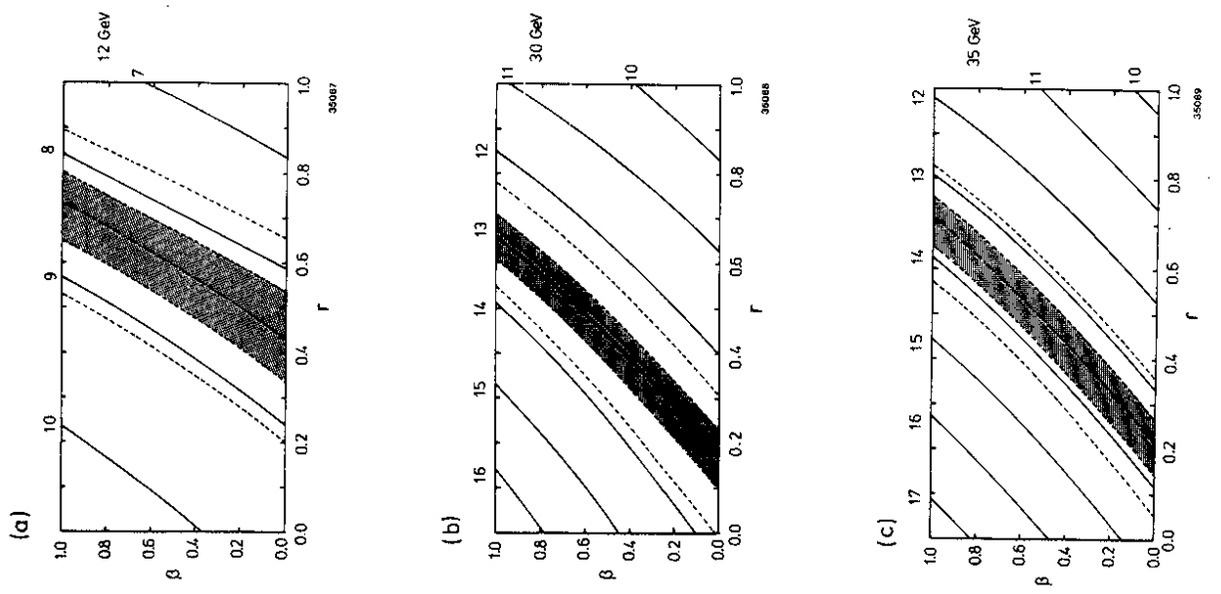
12 GeV
30 GeV
35 GeV
(a)
(b)
(c)
β
r
35087
35088
35089

Fig. 3

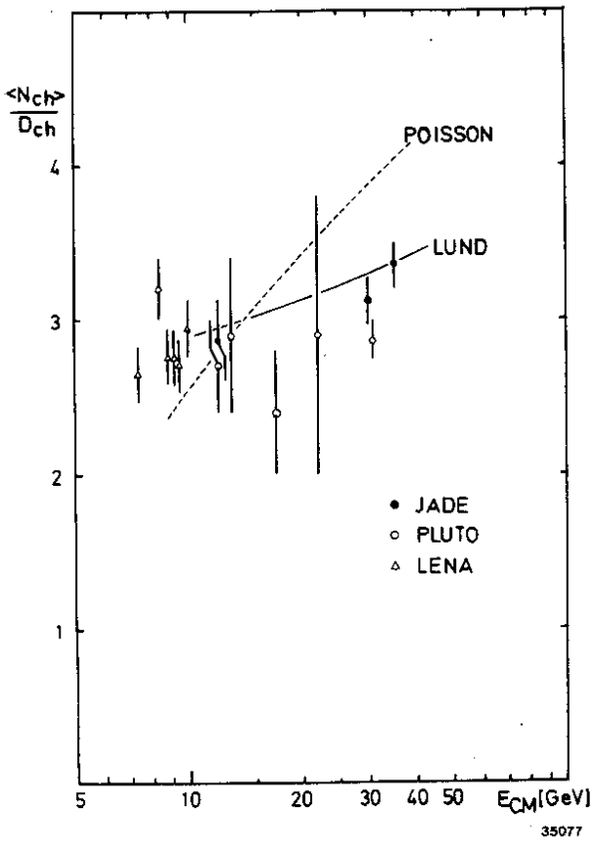

Fig. 6

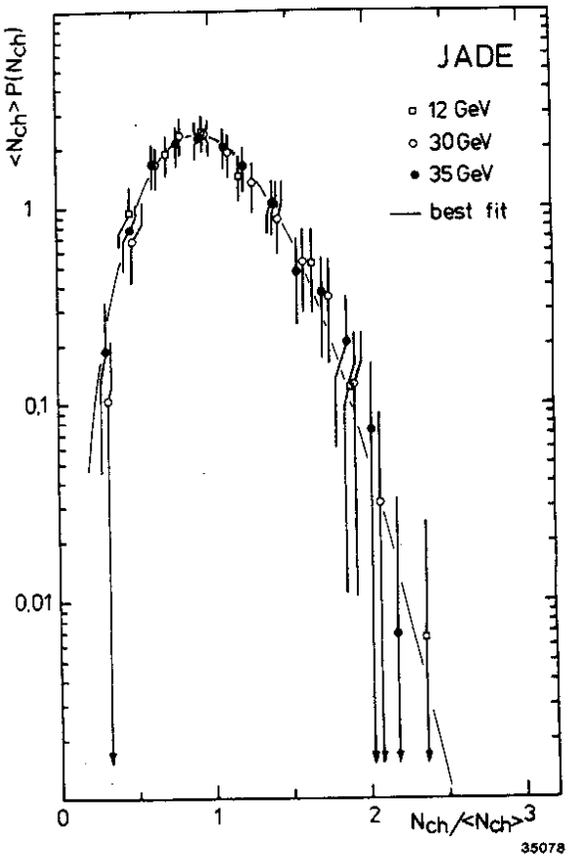

Fig. 7

Fig. 5

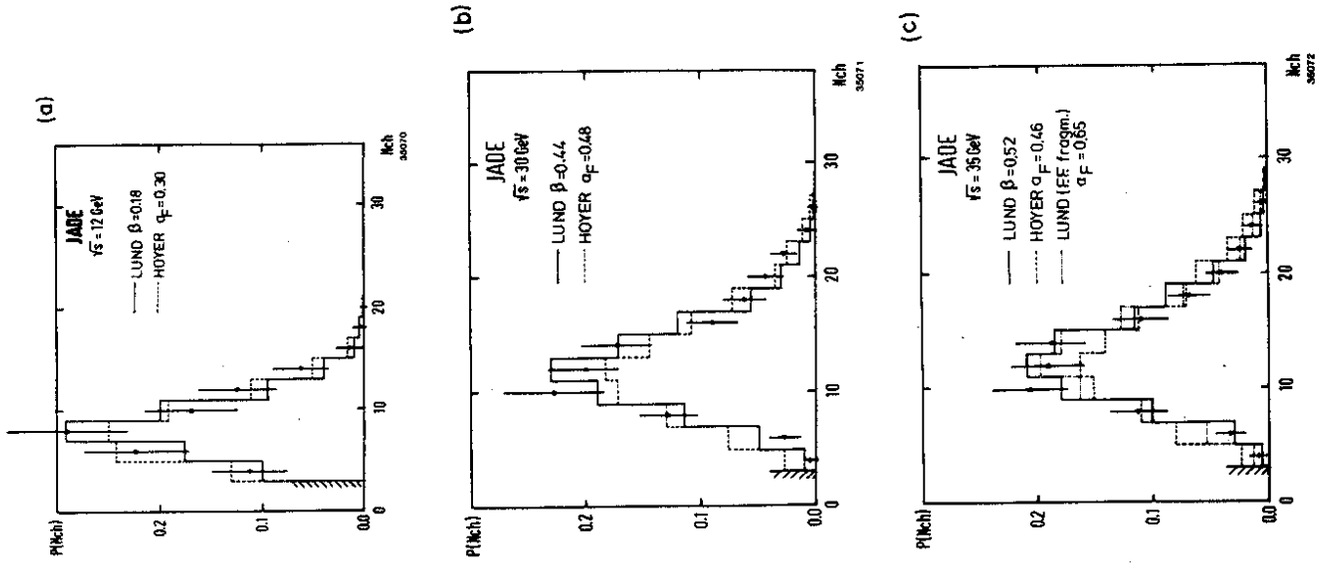

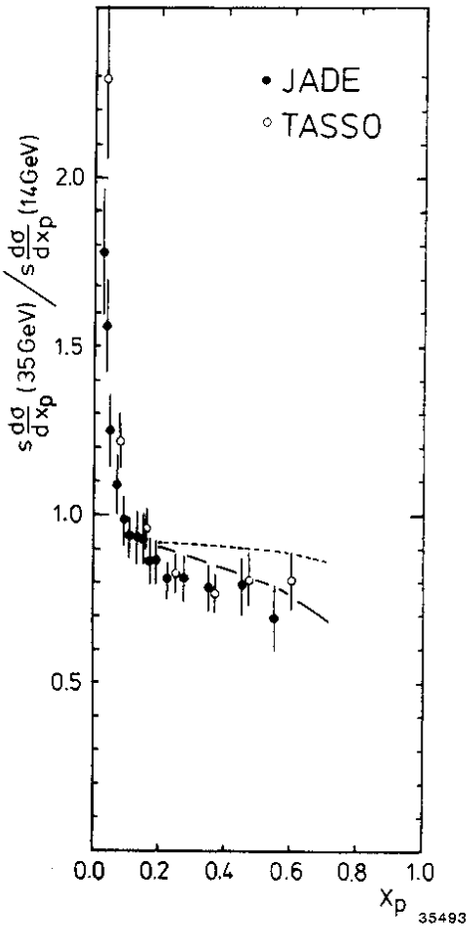

Fig. 9

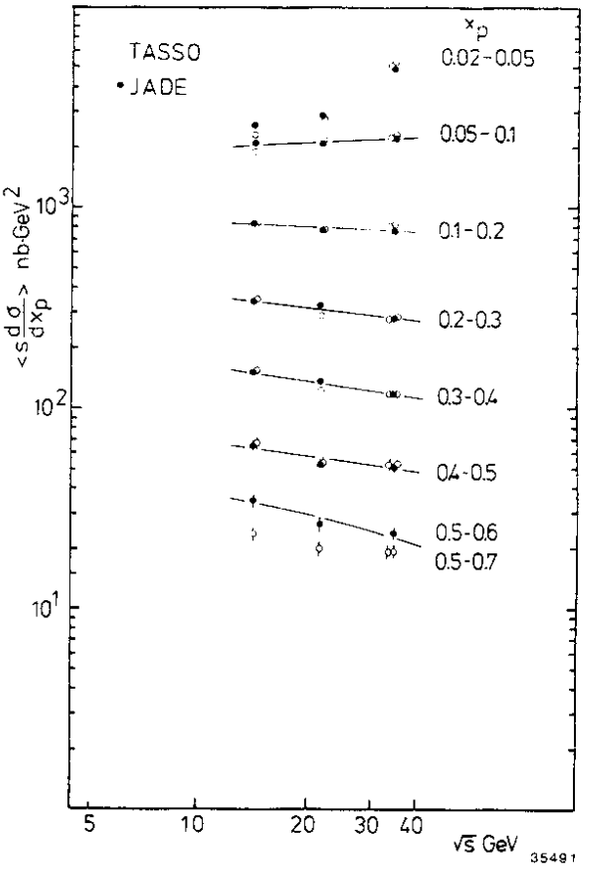

Fig.10

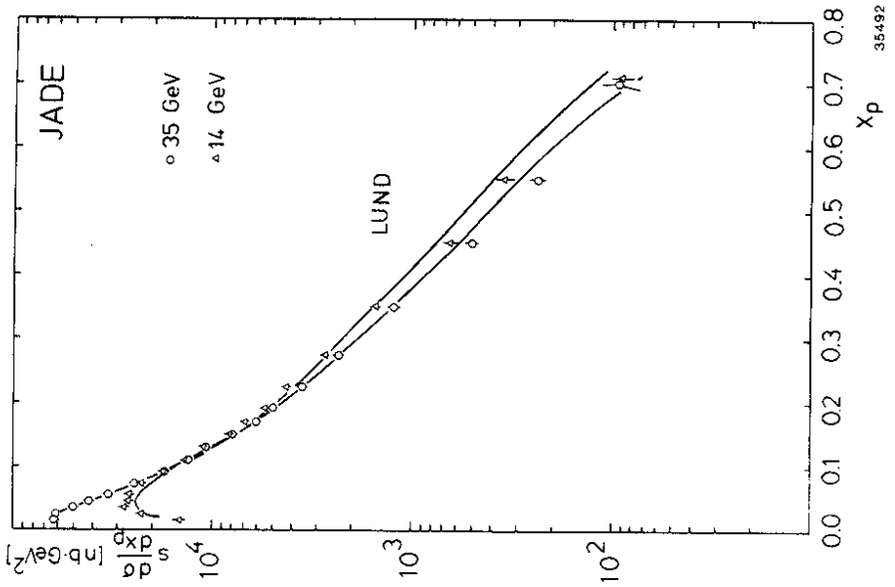

Fig. 8

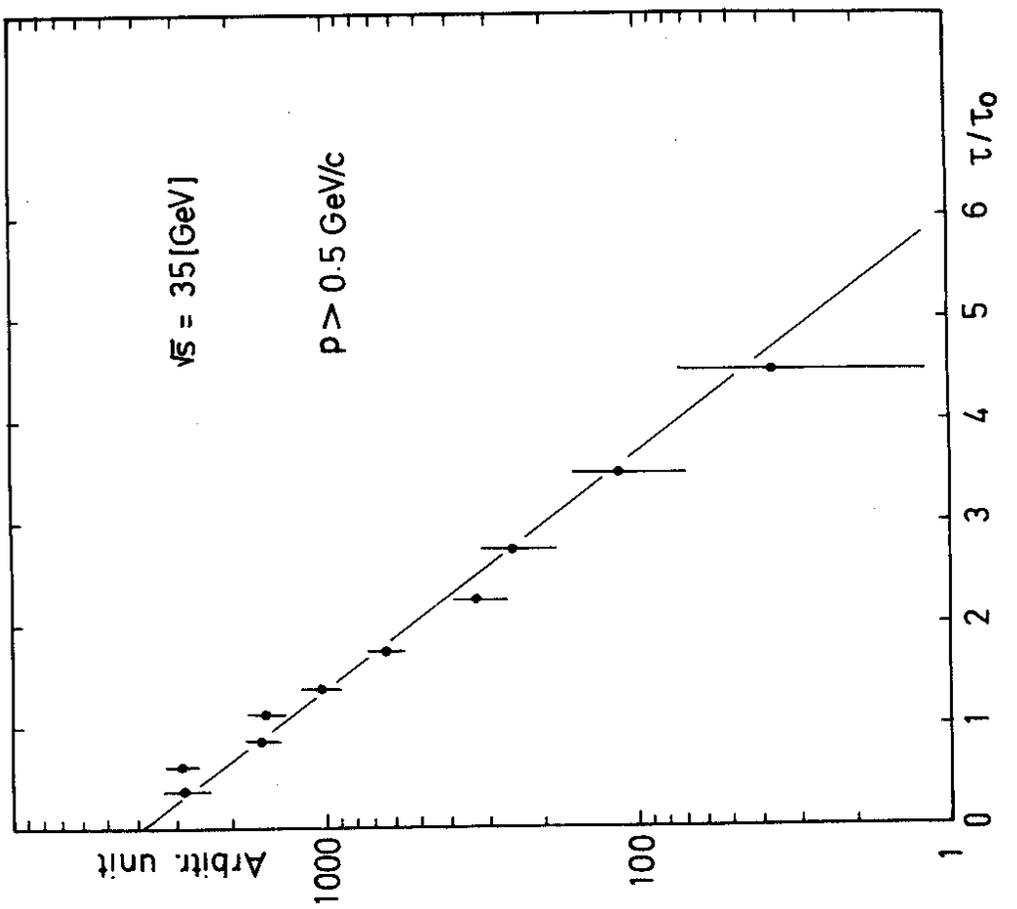
√s = 35 [GeV]
p > 0.5 GeV/c
Arbitr. unit
1000
100
1
0
1
2
3
4
5
6
τ/τ₀
35087

Fig.12

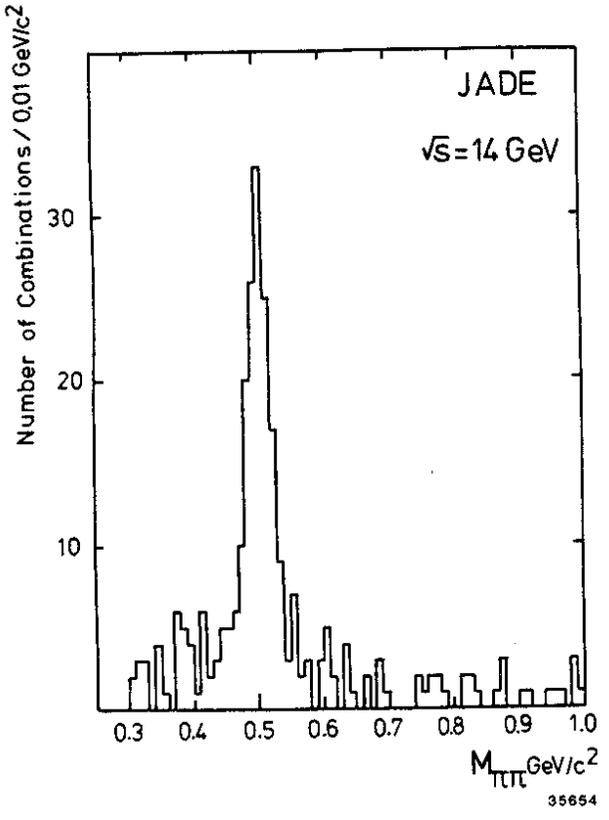
JADE
√s = 14 GeV
Number of Combinations / 0.01 GeV/c²
30
20
10
0.3
0.4
0.5
0.6
0.7
0.8
0.9
1.0
M_ππ GeV/c²
35654

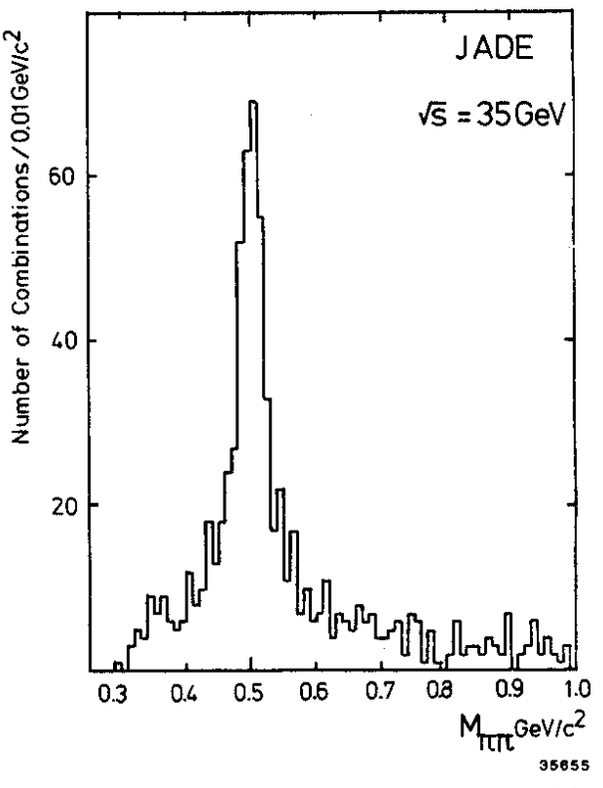
JADE
√s = 35 GeV
Number of Combinations / 0.01 GeV/c²
60
40
20
0.3
0.4
0.5
0.6
0.7
0.8
0.9
1.0
M_ππ GeV/c²
35655

Fig.11

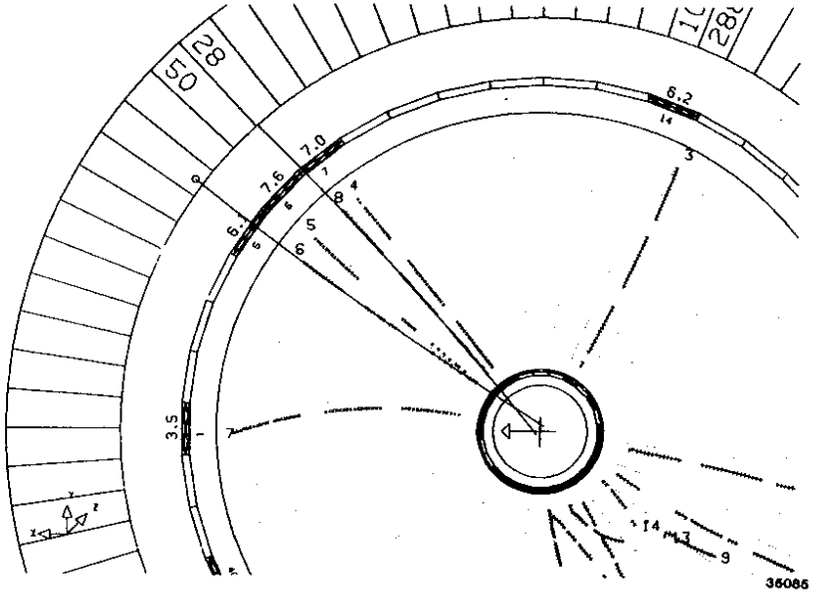

Fig.13

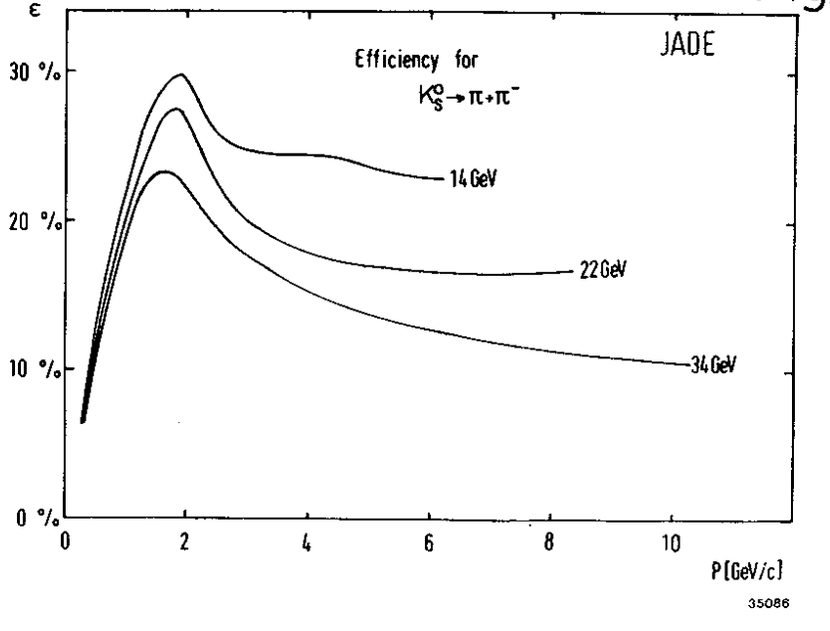

Fig.14

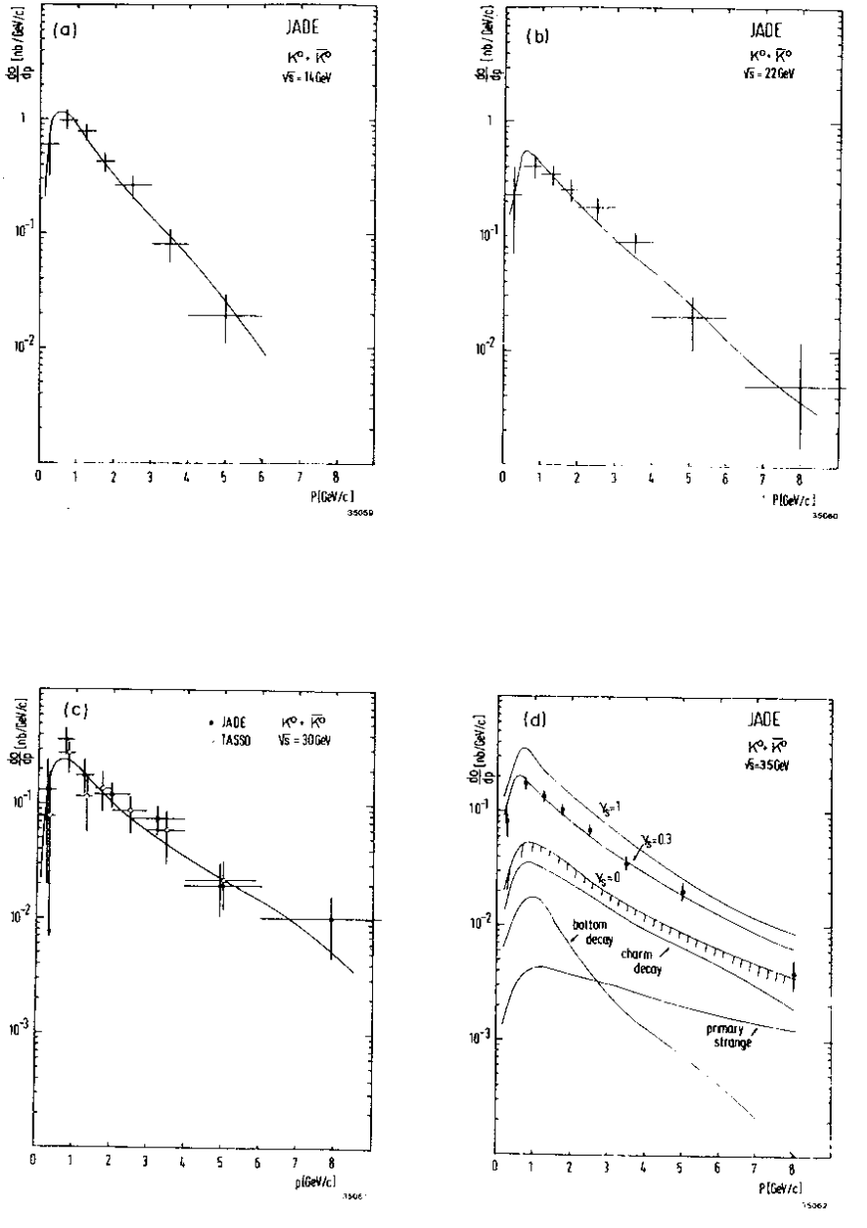

Fig.15

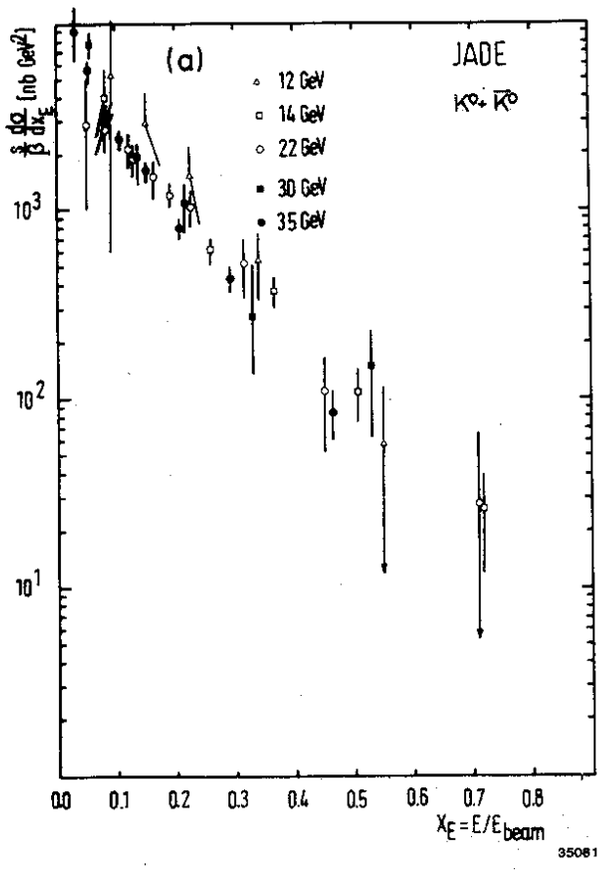
(a)
JADE
$K^0 + \bar{K}^0$
12 GeV
14 GeV
22 GeV
30 GeV
35 GeV
$\frac{s}{\beta} \frac{d\sigma}{dx_E}$ (nb GeV^2)
10^3
10^2
10^1
0.0 0.1 0.2 0.3 0.4 0.5 0.6 0.7 0.8
$X_E = E/E_{beam}$
35081

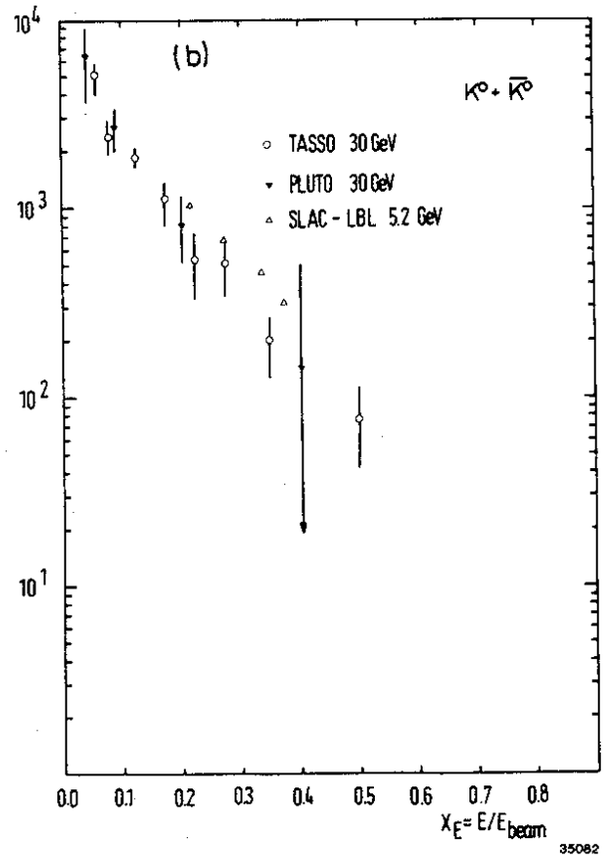
(b)
$K^0 + \bar{K}^0$
TASSO 30 GeV
PLUTO 30 GeV
SLAC - LBL 5.2 GeV
10^4
10^3
10^2
10^1
0.0 0.1 0.2 0.3 0.4 0.5 0.6 0.7 0.8
$X_E = E/E_{beam}$
35082

Fig.17

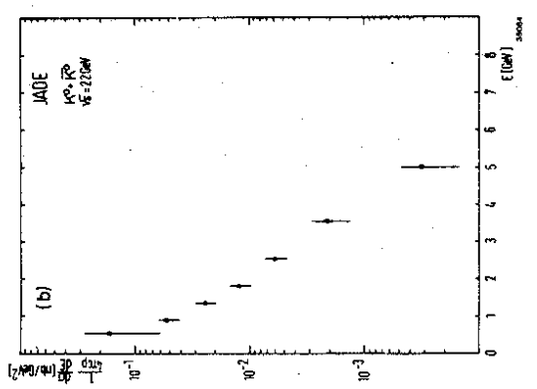
JADE
$K^0 + \bar{K}^0$
$\sqrt{s}$ = 22 GeV
(b)
E [GeV]

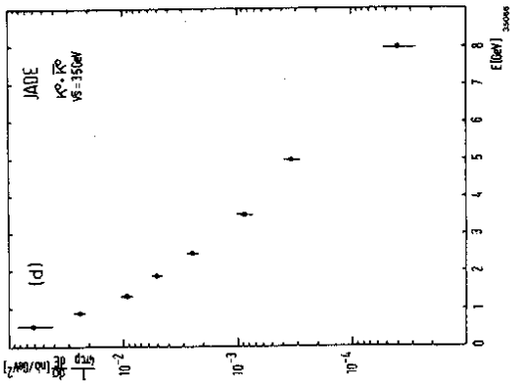
JADE
$K^0 + \bar{K}^0$
$\sqrt{s}$ = 35 GeV
(d)
E [GeV]

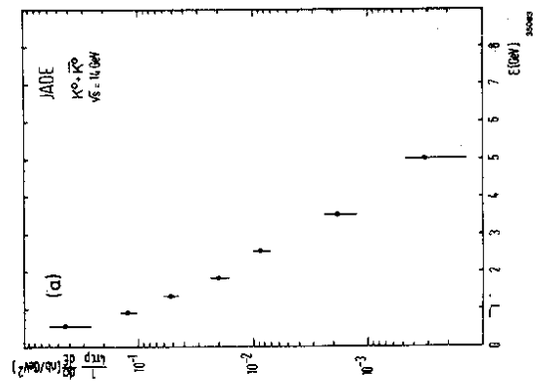
JADE
$K^0 + \bar{K}^0$
$\sqrt{s}$ = 14 GeV
(a)
E [GeV]

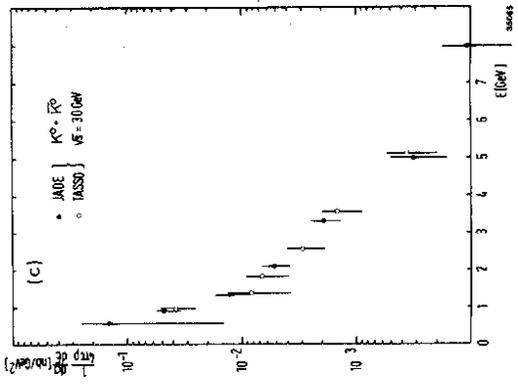
JADE
TASSO
$K^0 + \bar{K}^0$
$\sqrt{s}$ = 30 GeV
(c)
E [GeV]

Fig.16

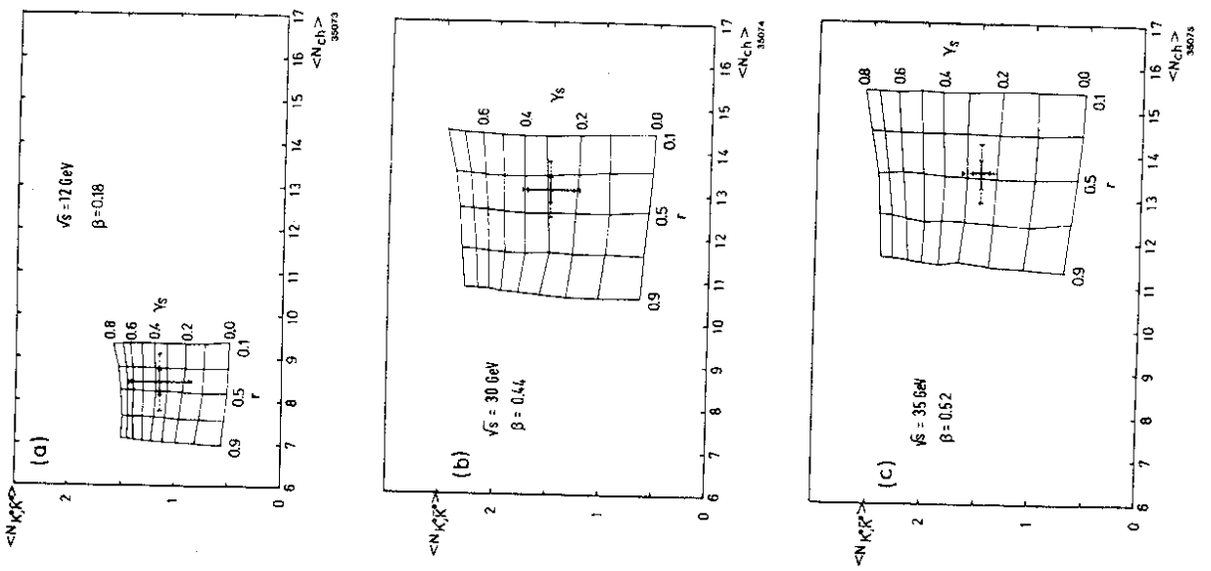
(a)
(b)
(c)
√s = 12 GeV
β = 0.18
√s = 30 GeV
β = 0.44
√s = 35 GeV
β = 0.52
Ys
r

Fig.19

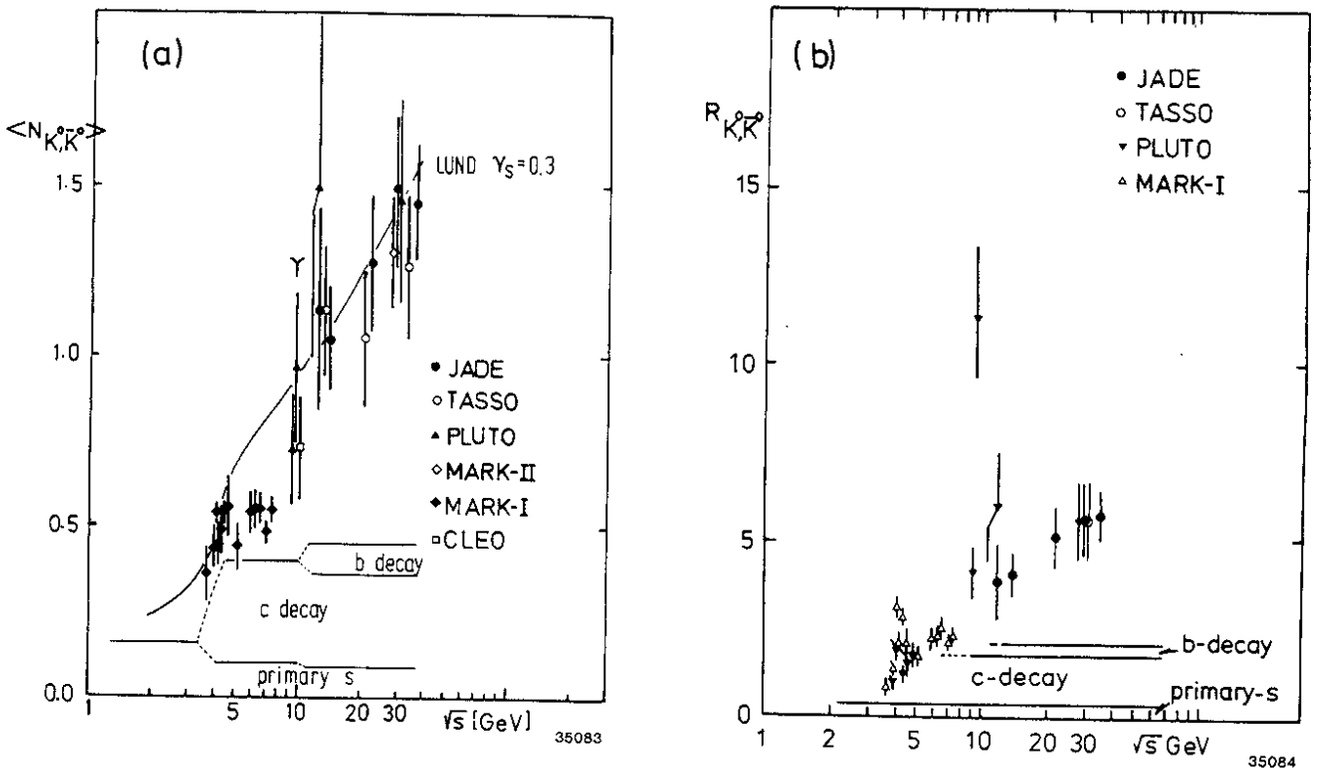
(a)
LUND Ys = 0.3
Υ
JADE
TASSO
PLUTO
MARK-II
MARK-I
CLEO
b decay
c decay
primary s
√s [GeV]
35083
(b)
JADE
TASSO
PLUTO
MARK-I
b-decay
c-decay
primary-s
√s GeV
35084

Fig.18

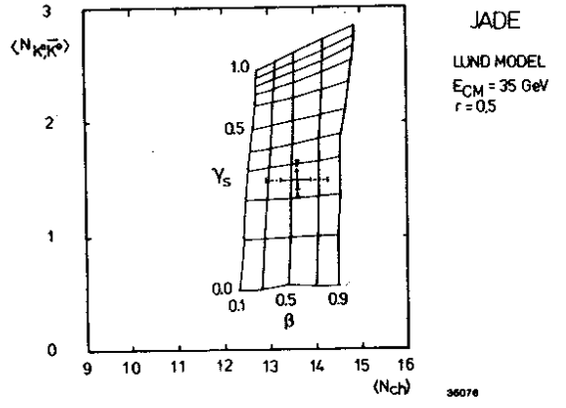
3
⟨N_K⁰K̄⁰⟩
2
1
0
9
10
11
12
13
14
15
16
⟨Nch⟩
1.0
0.5
Ys
0.0
0.1
0.5
0.9
β
JADE
LUND MODEL
E_CM = 35 GeV
r = 0.5
36076

Fig. 20